nature immunology

ARTICLES

https://doi.org/10.1038/s41590-019-0513-z

# Commensal viruses maintain intestinal intraepithelial lymphocytes via noncanonical RIG-I signaling

Lei Liu[1,3], Tao Gong[1,3], Wanyin Tao[1,3], Bolong Lin[1], Cong Li[1], Xuesen Zheng[1], Shu Zhu[1*], Wei Jiang[1*] and Rongbin Zhou[1,2*]

**Much attention has focused on commensal bacteria in health and disease, but the role of commensal viruses is understudied. Although metagenomic analysis shows that the intestine of healthy humans and animals harbors various commensal viruses and the dysbiosis of these viruses can be associated with inflammatory diseases, there is still a lack of causal data and underlying mechanisms to understand the physiological role of commensal viruses in intestinal homeostasis. In the present study, we show that commensal viruses are essential for the homeostasis of intestinal intraepithelial lymphocytes (IELs). Mechanistically, the cytosolic viral RNA-sensing receptor RIG-I in antigen-presenting cells can recognize commensal viruses and maintain IELs via a type I interferon–independent, but MAVS-IRF1-IL-15 axis-dependent, manner. The recovery of IELs by interleukin-15 administration reverses the susceptibility of commensal virus-depleted mice to dextran sulfate sodium–induced colitis. Collectively, our results indicate that commensal viruses maintain the IELs and consequently sustain intestinal homeostasis via noncanonical RIG-I signaling.**

The gut microbiota contains a vast number of microorganisms, including bacteria, fungi and viruses. Much attention has been focused on studying the dynamic interactions between commensal bacteria and the host immune system, which are critically involved in the development, function and homeostasis of gut-associated lymphoid tissues and various immune cell populations[1]. Metagenomic analysis shows that the intestine of healthy humans and animals harbors commensal viruses, such as DNA viruses or RNA viruses[2–5], the dysbiosis of which is often associated with inflammatory bowel diseases[6]. Moreover, there is evidence to show that commensal viruses can shape mucosal immunity. During tissue damage, commensal viruses can provide protection from pathological intestinal inflammation via induction of interferons (IFNs)[7,8]. In addition, when the commensal bacteria are absent, murine norovirus (MNV) can show a similar capacity to bacteria and restore intestinal lymphocyte number, and function in germ-free or antibiotic-treated mice via IFNs[9]. These results suggest that commensal viruses might compensate for alterations in commensal bacteria and exert a regulatory role on mucosal immunity without the presence of commensal bacteria; however, the physiological role and mechanism of commensal viruses in the development and homeostasis of intestinal lymphoid tissues and immune cells are unknown.

The intestinal immune system is considered the most complex part of host immune system, mainly comprising IELs, lamina propria lymphocytes (LPLs) and Peyer's patches (PPs)[10,11]. IELs are located in the intestinal epithelial layer and directly interact with intestinal epithelial cells (IECs), so they are close to antigens in the gut lumen[10,11]. IELs show different phenotypes with the lymphocytes in spleen, blood or lymph nodes and >70% of them are $CD8^+$ T cells. In particular, IELs contain greater numbers of T cell receptor (TCR)-$\gamma\delta^+$ T cells and $CD8\alpha\alpha^+$ T cells, the frequencies of which are very low in the circulation[12]. IELs show an 'innate' or 'memory-like' phenotype and play an important role in the homeostasis of intestinal mucosa[12], and their loss results in impaired host defense and increased susceptibility to tissue damage[13–15]. Notably, commensal bacteria have been reported to play a critical role in the homeostasis of IELs by producing pathogen-associated molecular patterns or metabolites, such as lipoteichoic acid, lipopolysaccharide, muramyl dipeptide or indole[16–20]. In contrast to commensal bacteria, the contribution of commensal viruses to the development and homeostasis of IELs is unknown.

In this study, we investigated the role of commensal viruses in the maintenance of IELs. Our study demonstrates that commensal viruses are essential for the homeostasis of $CD8\alpha\alpha^+$TCR-$\alpha\beta^+$ and $CD8\alpha\beta^+$TCR-$\alpha\beta^+$ IELs. Our data also indicate that RIG-I signaling in antigen-presenting cells (APCs) can recognize commensal viruses to maintain homeostasis of IELs, and prevent inflammation and tissue damage via a MAVS-IRF1-IL-15 axis.

## Results

**Commensal viruses maintain IELs.** To investigate the role of commensal viruses in the homeostasis of the intestinal immune system, we first conducted a metagenomic analysis of fecal virus-like particle (VLP)-derived DNA and RNA to identify commensal viruses colonizing specific pathogen-free (SPF) C57BL/6J mice. The intestinal virome contained viruses that infect both eukaryotic cells (eukaryotic viruses) and bacteria (bacteriophages) (see Supplementary Fig. 1a,b). For bacteriophages, Podoviridae, Siphoviridae, Myoviridae and Microviridae were the major family members (see Supplementary Fig. 1a,b). In addition, the intestinal

[1]Hefei National Laboratory for Physical Sciences at Microscale, CAS Key Laboratory of Innate Immunity and Chronic Disease, School of Basic Medical Sciences, Division of Life Science and Medicine, University of Science and Technology of China, Hefei, China. [2]CAS Centre for Excellence in Cell and Molecular Biology, University of Science and Technology of China, Hefei, China. [3]These authors contributed equally: Lei Liu, Tao Gong, Wanyin Tao. *e-mail: zhushu@ustc.edu.cn; ustcjw@ustc.edu.cn; zrb1980@ustc.edu.cn

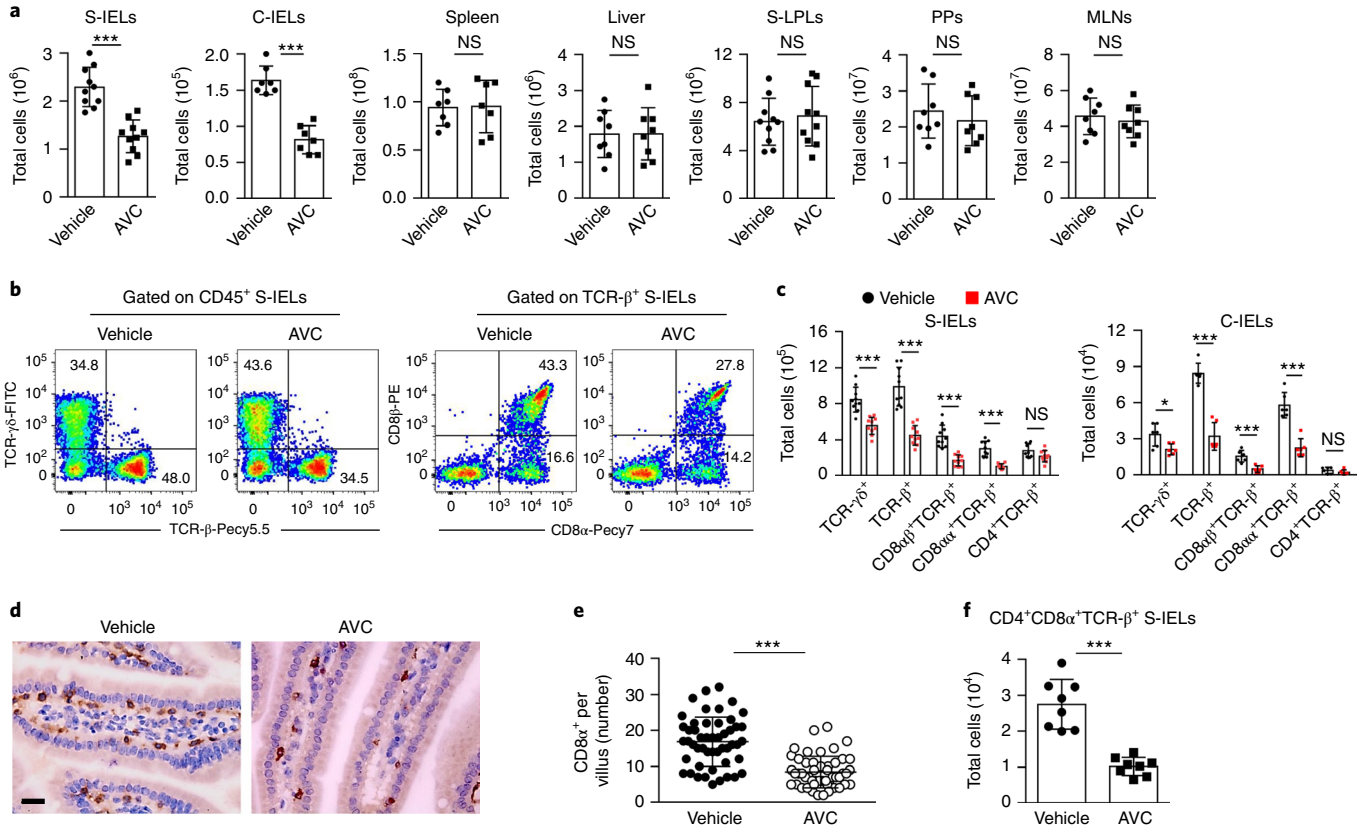


**Fig. 1 | Commensal viruses maintain IELs. a**, The number of S-IELs ($n=10$), colonic IELs (C-IELs) ($n=7$), small intestinal LPLs (S-LPLs) ($n=10$), lymphocytes from the spleen ($n=7$) and liver ($n=8$), PPs (n = 8) and MLNs ($n=8$) from vehicle- or AVC-treated mice. **b**, Flow cytometry analysis of S-IEL subsets from vehicle or AVC-treated mice. Numbers in the pseudocolor plots indicate the percentage of cells represented in the quadrant. **c**, The number of indicated S-IEL ($n=10$) or C-IEL ($n=6$) subsets from vehicle- or AVC-treated mice. **d**, Immunohistochemistry staining of tissue samples from the small intestine of AVC-treated mice with anti-CD8α antibodies (brown). Scale bars: 50 μm. **e**, Quantification of anti-CD8α staining in the villi of AVC-treated mice. Data were from 50 villi per sample. **f**, The number of $CD4^+CD8\alpha^+TCR\text{-}\beta^+$ S-IELs from vehicle- or AVC-treated mice ($n=8$). Data pooled from three independent experiments (**a**,**c**,**f**) or one experiment representative of at least two independent experiments (**b**,**d**,**e**) are shown (mean ± s.d.). The *P* values were determined using two-tailed, Student's *t*-tests (**a**,**c**,**e**,**f**). $^*P<0.05$, $^{**}P<0.01$, $^{***}P<0.001$. NS, not significant.

virome contained some eukaryotic virus family members, including both DNA and RNA viruses (see Supplementary Fig. 1a,b). MNV, a positive-strand RNA virus that is endemic in mouse facilities[21], did not colonize the mice in our facility (see Supplementary Fig. 1c). To evaluate the role of these viruses in the intestinal immune system, we then tried to deplete the commensal viruses in the gut by feeding C57BL/6J wild-type (WT) mice with an antiviral cocktail (AVC: ribavirin, lamivudine and aciclovir), starting at 2 weeks after birth. The numbers of fecal VLPs, including both DNA viruses and RNA viruses, are reduced notably after 6 weeks of treatment (see Supplementary Fig. 1d).

As the intestinal immune system mainly comprises IELs, LPLs, PPs and mesenteric lymph nodes (MLNs)[10,11,22], we then examined the effects of AVC treatment on the lymphocytes of these intestinal immune compartments. In AVC-treated mice, the numbers of IELs were reduced notably in both the small intestine and the colon (Fig. 1a). IELs are simply classified as $TCR\text{-}\gamma\delta^+$, $CD8\alpha\alpha^+TCR\text{-}\alpha\beta^+$, $CD8\alpha\beta^+TCR\text{-}\alpha\beta^+$ and $CD4^+TCR\text{-}\alpha\beta^+$ IELs[10,11]; we further analyzed the effects of commensal viruses on the subpopulations of IELs. $CD8\alpha\alpha^+TCR\text{-}\alpha\beta^+$ IELs and $CD8\alpha\beta^+TCR\text{-}\alpha\beta^+$ IELs were dramatically reduced, but the $TCR\text{-}\gamma\delta^+$ IELs and $CD4^+TCR\text{-}\alpha\beta^+$ IELs were slightly decreased or normal (Fig. 1b,c and see Supplementary Fig. 2a). The decrease in $CD8^+$ IELs was also confirmed by staining CD8α in sections of the small intestine or colon (Fig. 1d,e and see Supplementary Fig. 2b,c). Using TCR-δ–green fluorescent protein (GFP)-transgenic mice, we confirmed that AVC treatment slightly reduced the $TCR\text{-}\gamma\delta^+$ IELs of the small intestine (S-IELs) (see Supplementary Fig. 2d,e). In addition, the number of $CD4^+CD8\alpha^+TCR\text{-}\alpha\beta^+$ IELs was also decreased in the small intestine of AVC-treated mice (Fig. 1f).

As AVC treatment reduced both eukaryotic viruses and bacteriophages, we then asked which type of commensal viruses was involved in IEL homeostasis. As commensal bacteria are important for the maintenance of IELs, and bacteriophages live and replicate in commensal bacteria[16,23], we could not prove whether bacteriophages themselves had an impact on IEL homeostasis. However, we found that AVC treatment could further reduce IELs in the mice that have been treated with antibiotics to deplete commensal bacteria (see Supplementary Fig. 3a), suggesting that IEL homeostasis depends on eukaryotic viruses, at least in part.

Next we examined whether AVC treatment had an impact on the lymphocytes of other immune organs or compartments. In AVC-treated mice, the numbers of lymphocytes in the liver, spleen, lamina propria, PPs or MLNs were normal compared with vehicle-treated mice (Fig. 1a). Further analysis showed that commensal virus depletion had no effect on the percentages of the major immune cell subpopulations, including B, $CD4^+$ T, $CD8^+$ T, natural killer (NK) or NK T cells in the spleen, liver and MLNs (see Supplementary Fig. 3b,c). The percentages of effector memory ($T_{em}$) and central memory ($T_{cm}$) $CD8^+$ T cells were also normal in these compartments after AVC treatment (see Supplementary Fig. 3d). In PPs and the lamina propria, AVC treatment had no effect on the B

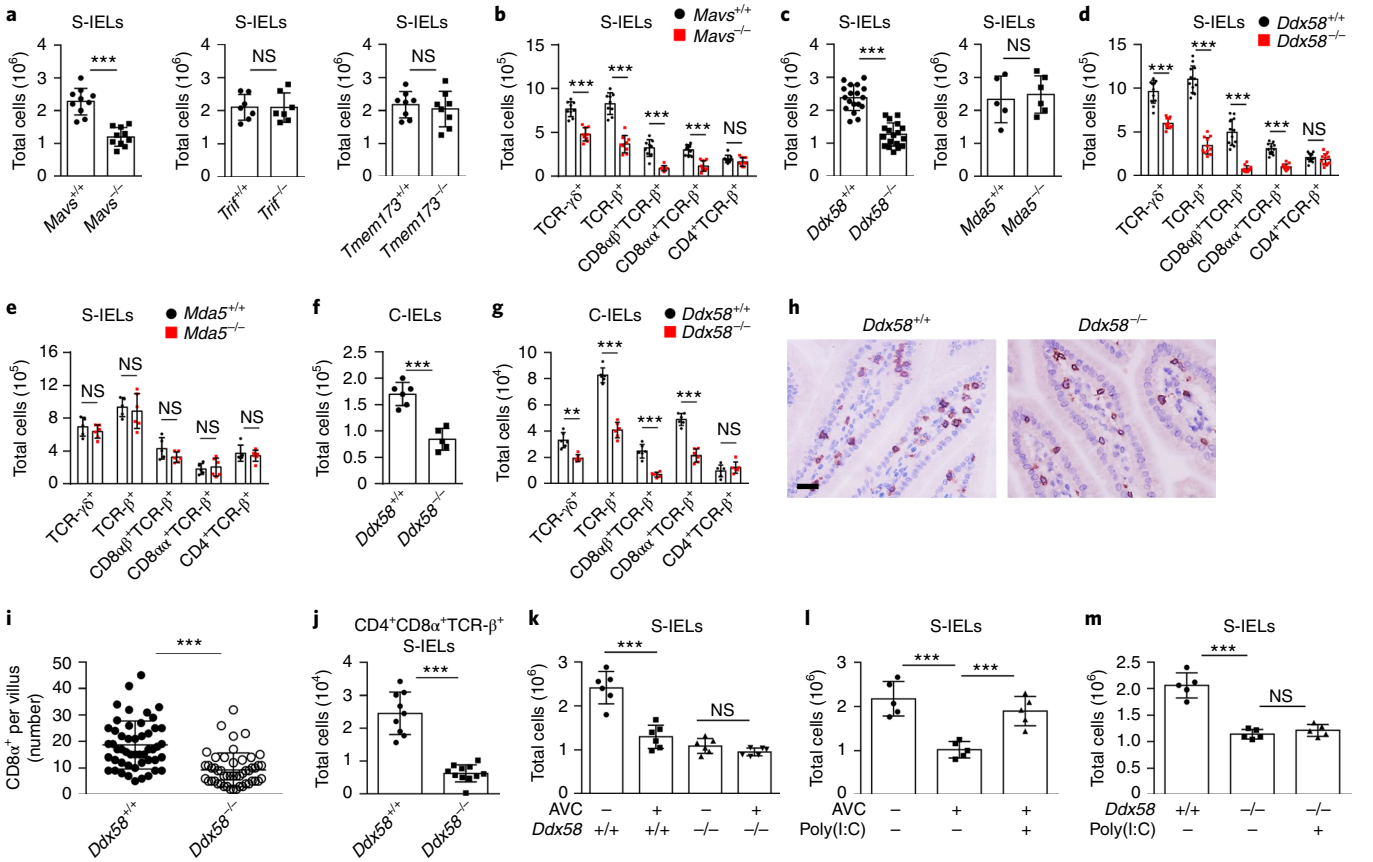


**Fig. 2 | RIG-I recognizes commensal viruses to maintain IELs. a**, The number of S-IELs from *Mavs*$^{-/-}$ mice ($n=10$), *Trif*$^{-/-}$ mice ($n=7$) and *Tmem173*$^{-/-}$ mice ($n=8$). **b**, The number of indicated S-IEL subsets from *Mavs*$^{+/+}$ or *Mavs*$^{-/-}$ mice ($n=9$). **c**, The number of S-IELs from *Ddx58*$^{-/-}$ ($n=18$) or *Mda5*$^{-/-}$ mice ($n=6$). **d**, The number of indicated S-IEL subsets from *Ddx58*$^{+/+}$ or *Ddx58*$^{-/-}$ mice ($n=12$). **e**, The number of indicated S-IEL subsets from *Mda5*$^{+/+}$ or *Mda5*$^{-/-}$ mice ($n=6$). **f**,**g**, The number of C-IELs (**f**) or indicated subsets (**g**) from *Ddx58*$^{+/+}$ or *Ddx58*$^{-/-}$ mice ($n=6$). **h**, Staining of tissue samples from the small intestine of *Ddx58*$^{+/+}$ or *Ddx58*$^{-/-}$ mice with anti-CD8α antibodies (brown). Scale bars: 50 μm. **i**, Quantification of anti-CD8α staining in the villi of *Ddx58*$^{+/+}$ or *Ddx58*$^{-/-}$ mice. Data were from 50 villi per sample. **j**, The number of CD4$^+$CD8α$^+$TCR-β$^+$ S-IELs from *Ddx58*$^{+/+}$ or *Ddx58*$^{-/-}$ mice ($n=9$). **k**, The number of S-IELs from *Ddx58*$^{+/+}$ or *Ddx58*$^{-/-}$ mice with or without AVC treatment ($n=6$). **l**, The number of S-IELs in mice treated with AVC alone or in the presence of PEI-encapsulated poly(I:C) ($n=5$). **m**, The number of S-IELs in *Ddx58*$^{+/+}$ or *Ddx58*$^{-/-}$ mice with or without the presence of PEI-encapsulated poly(I:C) ($n=5$). Data pooled from three independent experiments (**a**–**g**,**j**), two independent experiments (**k**–**m**) and one experiment representative of at least two independent experiments (**h**,**i**) are shown (mean ± s.d.). The *P* values were determined using two-tailed, Student's *t*-tests (**a**,**g**,**i**,**j**) or one-way ANOVA for multiple comparisons (**k**–**m**). $^*P<0.05$, $^{**}P<0.01$, $^{***}P<0.001$.

and CD4$^+$ T cells, but deceased the numbers of CD103$^+$CD8$^+$ T cells (see Supplementary Fig. 3e,f), which are tissue-resident memory T cells in the intestine[24]. Thus, these results suggest that commensal viruses are critical for maintenance of the homeostasis of IELs.

**RIG-I recognizes commensal viruses to maintain IELs.** We then investigated the mechanism of how commensal viruses maintain IELs. The major pattern recognition receptors detecting viral components include toll-like receptors (TLRs), RIG-I-like receptors and cyclic GMP–AMP synthase (cGAS), which can initiate antiviral immune responses via the adapter proteins TRIF, mitochondrial antiviral-signaling (MAVS) protein and stimulator of interferon genes (STING), respectively[25]. The analysis of *Mavs*$^{-/-}$ mice showed that these mice exhibited a similar phenotype to AVC-treated mice and the number of S-IELs, especially the CD8αα$^+$TCR-αβ$^+$ and CD8αβ$^+$TCR-αβ$^+$ IELs, was notably decreased in *Mavs*$^{-/-}$ mice, but normal in *Trif*$^{-/-}$(also known as *Ticam1*$^{-/-}$) and STING-deficient (*Tmem173*$^{-/-}$) mice (Fig. 2a,b). In contrast, the number of lymphocytes in the liver, spleen and LPLs was not altered in *Mavs*$^{-/-}$ mice (see Supplementary Fig. 4a). Both RIG-I and MDA5 can recognize that viral RNA derived from RNA and DNA viruses activates downstream signaling via MAVS[26]; the IELs in RIG-I deficient (*Ddx58*$^{-/-}$) and *Mda5*$^{-/-}$ mice were then analyzed. Similar to AVC-treated mice, the numbers of CD8αα$^+$TCR-αβ$^+$ and CD8αβ$^+$TCR-αβ$^+$ IELs were notably decreased in the small intestine of *Ddx58*$^{-/-}$ mice, whereas *Mda5*$^{-/-}$ mice were normal (Fig. 2c–e). The similar IEL loss was also observed in the colon of *Ddx58*$^{-/-}$ mice (Fig. 2f,g). In addition the decrease in CD8$^+$ IELs was confirmed by staining of CD8α in sections of the small intestine or colon in *Ddx58*$^{-/-}$ mice (Fig. 2h,i and see Supplementary Fig. 4b,c). In addition, the numbers of CD4$^+$CD8α$^+$TCR-β$^+$ IELs were decreased in the small intestine of *Ddx58*$^{-/-}$ mice (Fig. 2j).

To further confirm that commensal viruses maintain IELs via RIG-I signaling, we fed *Ddx58*$^{-/-}$ mice AVC and found that commensal virus depletion had no impact on the IELs in *Ddx58*$^{-/-}$ mice (Fig. 2k). However, antibiotic treatment could further reduce IELs in *Ddx58*$^{-/-}$ mice (see Supplementary Fig. 4d). Moreover, intraperitoneal supplementation of poly(I:C) encapsulated with polyethylenimine (PEI), a ligand for RIG-I, could rescue the IEL loss in AVC-treated *Ddx58*$^{+/+}$ mice (Fig. 2l), but not in *Ddx58*$^{-/-}$ mice (Fig. 2m). In contrast, supplementation of poly(A:T) could not rescue the IEL loss in AVC-treated WT mice (see Supplementary

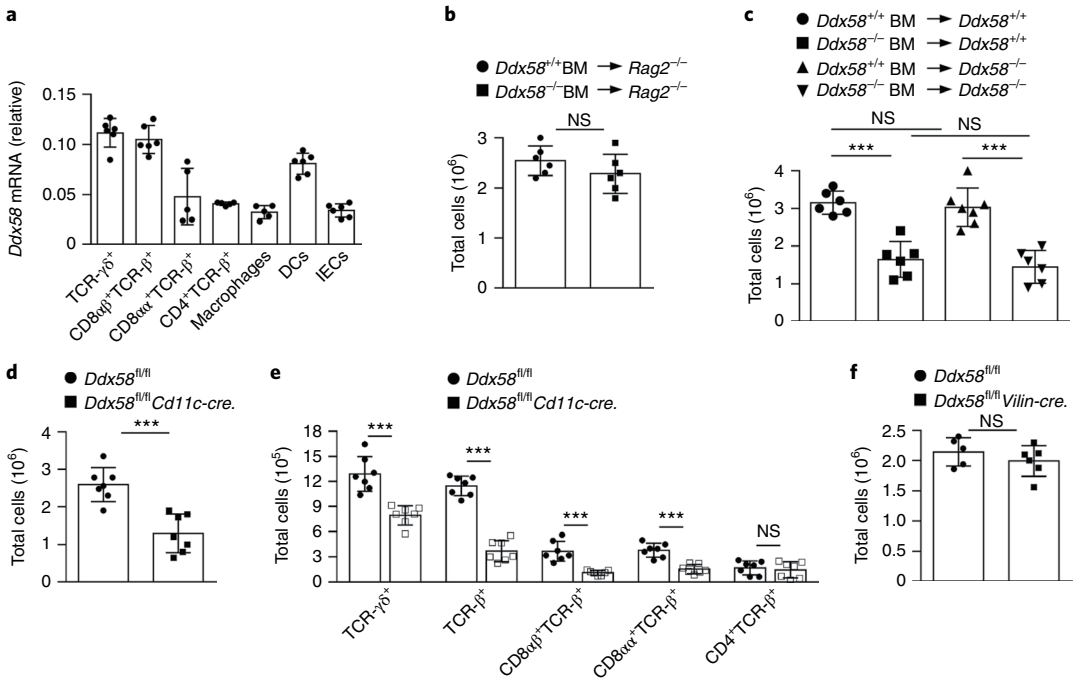


**Fig. 3 | RIG-I signaling in APCs maintains IELs. a**, Quantification of Ddx58 mRNA by quantitative (q)PCR in the indicated cell subsets (TCR-γδ$^+$ IELs, CD8αβ$^+$TCR-β$^+$ IELs, DCs, IECs, $n=6$; CD8αα$^+$TCR-β$^+$ IELs, CD4$^+$TCR-β$^+$ IELs, macrophages, $n=5$). **b**, The number of total S-IELs of the indicated BM chimeras in which *Ddx58*$^{+/+}$ or *Ddx58*$^{-/-}$ BM cells were transferred into irradiated *Rag2*$^{-/-}$ mice ($n=6$). **c**, The number of total S-IELs of the indicated BM chimeras in which *Ddx58*$^{+/+}$ BM cells were transferred into irradiated *Ddx58*$^{+/+}$ mice ($n=6$) or *Ddx58*$^{-/-}$ mice ($n=7$), or *Ddx58*$^{-/-}$ BM cells were transferred into irradiated *Ddx58*$^{+/+}$ mice ($n=6$) or *Ddx58*$^{+/+}$ mice ($n=6$). **d**,**e**, The number of the total S-IELs (**d**) and indicated subsets (**e**) from *Ddx58*$^{fl/fl}$*Cd11c-cre* or *Ddx58*$^{fl/fl}$ mice ($n=7$). **f**, The number of the total S-IELs from *Ddx58*$^{fl/fl}$*Villin-cre* mice ($n=6$) or *Ddx58*$^{fl/fl}$ mice ($n=5$). Data pooled from three independent experiments (**b**–**f**) or two independent experiments (**a**) are shown (mean ± s.d.). The *P* values were determined using two-tailed, Student's *t*-tests (**b**,**d**–**f**) or one-way ANOVA for multiple comparisons (**c**). $^*P<0.05$, $^{**}P<0.01$, $^{***}P<0.001$.

Fig. 4e). These results suggest that RIG-I recognizes commensal virus-derived RNA as maintaining IELs.

We next examined whether RIG-I signaling affected the lymphocytes of other immune organs or compartments. The number of lymphocytes in the thymus, liver, spleen, lamina propria, PPs or MLNs were normal in *Ddx58*$^{-/-}$ mice (see Supplementary Fig. 4f). The percentages of B cells, CD4$^+$ T cells, CD8$^+$ T, NK cells, NK T cells, $T_{em}$ CD8$^+$ T cells or $T_{cm}$ CD8$^+$ T cells in the spleen, liver and MLNs were also not changed in *Ddx58*$^{-/-}$ mice (see Supplementary Fig. 4g,h). In PPs and the lamina propria, the B and CD4$^+$ T cells were normal, but the memory CD103$^+$CD8$^+$ T cells were decreased in *Ddx58*$^{-/-}$ mice (see Supplementary Fig. 4i,j). Thus, commensal viruses maintain the homeostasis of IELs via RIG-MAVS signaling.

**RIG-I signaling on APCs maintains IELs.** We further investigated whether IEL-intrinsic or -extrinsic RIG-I signaling was responsible for the homeostasis of IELs, because RIG-I was widely expressed on IELs, macrophages, dendritic cells (DCs) and IECs (Fig. 3a). Adoptive transfer of bone marrow (BM) cells from RIG-I-sufficient (*Ddx58*$^{+/+}$) mice and RIG-I-deficient (*Ddx58*$^{-/-}$) mice both reconstituted IELs in *Rag2*-deficient hosts (Fig. 3b), suggesting that IEL-intrinsic RIG-I signaling is not required for the homeostasis of IELs. When BM cells from *Ddx58*$^{+/+}$ mice were transferred into lethally irradiated *Ddx58*$^{+/+}$ and *Ddx58*$^{-/-}$ mice, there was no difference for the reconstitution of IELs after 8 weeks (Fig. 3c), suggesting that RIG-I signaling in parenchymal cells, including IECs, is not responsible for the homeostasis of IELs. When BM cells from *Ddx58*$^{+/+}$ and *Ddx58*$^{-/-}$ mice were transferred into lethally irradiated *Ddx58*$^{+/+}$ mice, IELs in mice transferred with *Ddx58*$^{-/-}$ BM cells were poorly reconstituted compared with mice transferred with *Ddx58*$^{+/+}$ BM cells (Fig. 3c), suggesting that RIG-I signaling in hematopoietic cells is required for the homeostasis of IELs. As IEL-intrinsic RIG-I signaling was not involved (Fig. 3b), these results indicate that RIG-I signaling in the hematopoietic system–derived APCs, such as macrophages or DCs, might be critical for the homeostasis of IELs. To further confirm this, we constructed a conditional *Ddx58* knockout mice (*Ddx58*$^{fl/fl}$) (see Supplementary Fig. 5a). As both intestinal macrophages and DCs express CD11c[27], the mice were crossed with *Cd11c-cre* mice to delete RIG-I expression in both macrophages and DCs (see Supplementary Fig. 5b). Consistent with global RIG-I-deficient mice, the numbers of IELs in *Ddx58*$^{fl/fl}$*Cd11c-cre* mice, especially the CD8αα$^+$TCR-αβ$^+$ and CD8αβ$^+$TCR-αβ$^+$ IELs, were notably decreased (Fig. 3d,e). In contrast, when the mice were crossed with *Villin-cre* (*Villin*, also known as *Vil1*) mice to delete RIG-I expression in IECs, the IELs were normal in *Ddx58*$^{fl/fl}$*Villin-cre* mice (see Supplementary Fig. 5c and Fig. 3f). These results indicate that the RIG-I signaling in APCs is responsible for the IEL homeostasis.

**RIG-I signaling maintains IELs independently of microbiota dysbiosis.** As commensal virus depletion and RIG-I deficiency can cause the dysbiosis of microbiota, which may result in the loss of IELs[7,28], we then investigated whether the IEL loss in *Ddx58*$^{-/-}$ mice was caused by the dysbiosis of microbiota. As expected, UniFrac-based principal-component analysis (PCA) showed that AVC treatment notably changed the bacterial community in the fecal samples of WT mice (Fig. 4a). Compared with control mice, AVC treatment resulted in decreased species diversity (Fig. 4b,c) and altered bacterial taxonomic composition (Fig. 4d,e) in fecal samples. In addition,

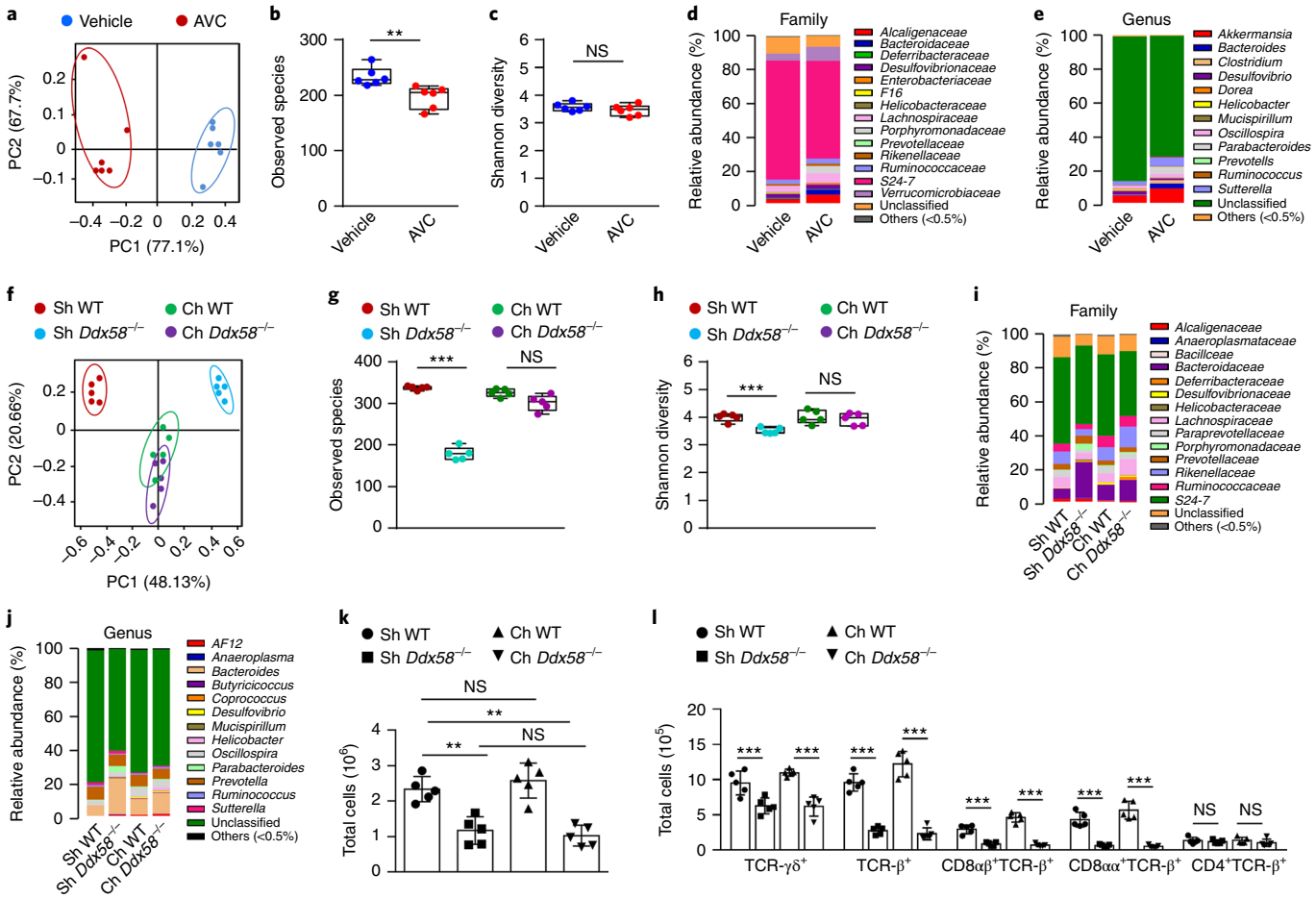


**Fig. 4 | RIG-I signaling maintains IELs independently of microbiota dysbiosis. a**, PCA plot generated from unweighted UniFrac distance matrix displaying the distinct clustering pattern of intestinal bacteria community in vehicle- or AVC-treated mice ($n=6$). **b**,**c**, The observed species number (**b**) and Shannon diversity index (**c**) of intestinal bacteria in vehicle- or AVC-treated mice ($n=6$). **d**,**e**, Relative abundance of taxonomic groups averaged across vehicle- or AVC-treated mice ($n=6$). **f**, PCA plot generated from unweighted UniFrac distance matrix displaying the distinct clustering pattern of intestinal bacteria community in single-housed (Sh) or co-housed (Ch) *Ddx58*$^{-/-}$ and WT mice ($n=5$). **g**,**h**, The observed species number (**g**) and Shannon diversity (**h**) index of intestinal bacteria in Sh or Ch *Ddx58*$^{-/-}$ and WT mice ($n=5$). **i**,**j**, Relative abundance of taxonomic groups averaged across Sh or Ch *Ddx58*$^{-/-}$ and WT mice ($n=5$). **k**,**l**, The number of the total S-IELs (**k**) and indicated subsets (**l**) from Sh or Ch *Ddx58*$^{-/-}$ and WT mice ($n=5$). Data from two independent experiments (**k**,**l**) are shown (mean ± SD). The *P* values were determined using two-tailed, Student's *t*-tests (**b**,**c**,**l**) or one-way ANOVA for multiple comparisons (**g**,**h**,**k**). $^{*}P<0.05$, $^{**}P<0.01$, $^{***}P<0.001$.

*Ddx58*$^{-/-}$ mice also showed a different composition of commensal bacteria and decreased species diversity, compared with WT mice (Fig. 4f–j). Furthermore, co-housing of *Ddx58*$^{-/-}$ mice with WT mice for 4 weeks synchronized their bacterial microbiome in the gut (Fig. 4f–j). However, the IELs were notably decreased in *Ddx58*$^{-/-}$ mice even in this condition (Fig. 4k,l), suggesting that the IEL loss in *Ddx58*$^{-/-}$ mice was not caused by the dysbiosis of microbiota.

**RIG-I signaling supports IEL proliferation and survival.** We next asked how APC-derived RIG-I signaling regulated the homeostasis of IELs. Although early studies implicate that IELs can develop extrathymically, more recent studies indicate that they are derived from thymic precursors, at least in the presence of a thymus[29]. Next we investigated whether RIG-I-MAVS signaling had an impact on the development of IELs in the thymus. CD8αα$^{+}$TCR-αβ$^{+}$ IELs are derived from CD4$^{-}$CD8$^{-}$NK1.1$^{-}$TCR-αβ$^{+}$ thymocytes, which can give rise to CD8αα$^{+}$TCR-αβ$^{+}$ IELs when transferred into *Rag2*$^{-/-}$ mice[30]. The results showed that CD4$^{-}$CD8$^{-}$NK1.1$^{-}$TCR-αβ$^{+}$ thymocytes were present in normal frequencies in *Mavs*$^{-/-}$ mice (Fig. 5a). Consistent with this, the numbers and frequencies of CD8$^{+}$ memory T cells in the spleen were normal (Fig. 5b). These results suggest that commensal viruses and RIG-MAVS signaling are not required for the development of IELs in thymus.

To further explore the reason for IEL loss, we examined whether RIG-I deletion affected the proliferation and apoptosis of IELs. The apoptosis and proliferation of IELs were analyzed by annexin-V staining and use of bromodeoxyuridine (BrdU) incorporation, respectively. CD8αα$^{+}$TCR-αβ$^{+}$ and CD8αβ$^{+}$TCR-αβ$^{+}$ IELs showed poorer proliferation and higher apoptosis in *Ddx58*$^{-/-}$ mice, whereas the TCR-γδ$^{+}$ IELs showed slightly higher apoptosis and lower proliferation, and the CD4$^{+}$TCR-αβ$^{+}$ IELs were normal (Fig. 5c,d). These results were consistent with the IEL loss in *Ddx58*$^{-/-}$ and commensal virus-depleted mice, suggesting that commensal viruses and RIG-I signaling regulate the homeostasis of IELs by regulating their proliferation and survival.

**Commensal viruses and RIG-I promote IL-15 production in APCs to maintain IELs.** To further investigate how APC-derived RIG-I signaling supports the proliferation and survival of IELs, we first tested the percentages and numbers of macrophages or DCs in LPLs in both WT and *Ddx58*$^{-/-}$ mice. The results showed that the percentages and number of macrophages or DCs in LPLs were

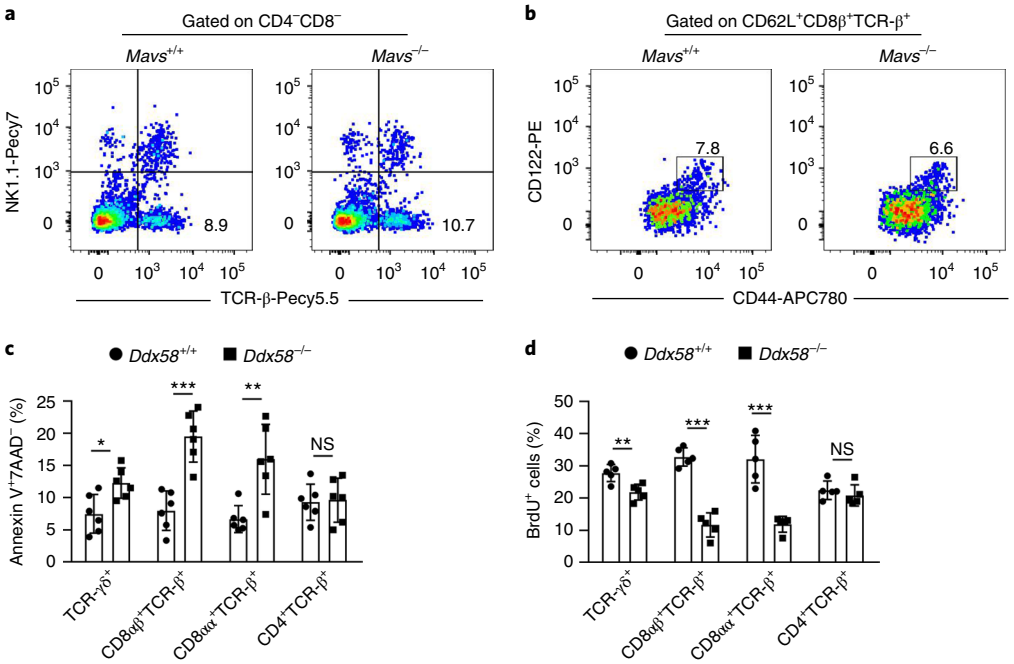


**Fig. 5 | RIG-I signaling supports IEL proliferation and survival. a**, Flow cytometry analysis of putative thymic IEL precursors in *Mavs*$^{+/+}$ or Mavs$^{-/-}$ mice. CD4$^-$CD8$^-$ thymocytes were analyzed for NK1.1 and TCR-β expression. Numbers in the quadrants indicate percentages. **b**, The splenocytes from *Mavs*$^{+/+}$ or Mavs$^{-/-}$ mice were stained as indicated. The percentages of memory CD8$^+$ T cells were shown. **c**, Quantification of the percentage of apoptotic (annexin-V$^+$7AAD$^-$) IEL subsets by flow cytometry in *Ddx58*$^{+/+}$ or *Ddx58*$^{-/-}$ mice ($n=6$). **d**, Quantification of the BrdU$^+$ IEL subsets by flow cytometry in *Ddx58*$^{+/+}$ or *Ddx58*$^{-/-}$ mice ($n=5$). Data from one experiment representative of at least two independent experiments (**a**,**b**) or two independent experiments (**c**,**d**) are shown (mean ± s.d.). The *P* values were determined using two-tailed Student's *t*-tests (**c**,**d**). $^*P<0.05$, $^{**}P<0.01$, $^{***}P<0.001$.

normal in *Ddx58*$^{-/-}$mice (see Supplementary Fig. 6a–d), suggesting that RIG-I signaling has no impact on the development of intestinal macrophages or DCs, and might maintain IELs via regulation of the function of APCs.

Commensal viruses and RIG-I signaling have been reported to protect tissue damage via promotion of the production of type I and type III IFNs[7,8,31]; we speculated that IFNs might be involved in the homeostasis of IELs. First, we examined the expression of IFN-α, -β or -λ in intestinal macrophages, DCs and IECs and found that RIG-I deficiency reduced their expression in intestinal macrophages and DCs, but not in IECs (Fig. 6a). We also examined the expression of the genes encoding receptors for IFN-α/β or IFN-λ (*Ifnar1* and *Ifnlr*, respectively) and found that APCs or IEL subsets highly expressed *Ifnar1*, whereas the expression of *Ifnlr* was extremely low (Fig. 6b), which is consistent with a previous report[8], suggesting that IFN-α/β might be involved in IEL homeostasis. We then analyzed *Ifnar1*$^{-/-}$ mice and found that IELs were normal in these mice (Fig. 6c). Moreover, intraperitoneal supplementation with poly(I:C) could still rescue the IEL loss in AVC-treated *Ifnar1*$^{-/-}$ mice (Fig. 6d). Thus, these results suggest that commensal viruses and APC-derived RIG-I signaling maintain IELs in a type I interferon (IFN-I)-independent manner.

Several cytokines, including transforming growth factor (TGF)-β, interleukin (IL)-15 and IL-7, have been reported to play an essential role in the differentiation, development and survival of IELs[19,32,33], so we examined whether commensal viruses and RIG-I signaling regulated the production of these cytokines to maintain IELs. The results showed that the APCs from *Ddx58*$^{-/-}$ mice expressed a much lower level of IL-15, but comparable levels of TGF-β and IL-7 (Fig. 6e and see Supplementary Fig. 7a,b). Indeed, IL-15 was highly expressed on both DCs and macrophages (Fig. 6f). IL-15 was also expressed on IECs, but its expression was independent of RIG-I signaling (Fig. 6g). Furthermore, we found that adeno-associated virus (AAV)-mediated gene delivery could restore the number of IELs in *Ddx58*$^{-/-}$ mice (Fig. 6h and see Supplementary Fig. 7c), suggesting that the impaired expression of IL-15 in APCs is responsible for the loss of IELs in *Ddx58*$^{-/-}$ mice. Similarly with *Ddx58*$^{-/-}$ mice, the APCs from commensal virus-depleted mice also expressed much lower IL-15 levels, and restoration of IL-15 expression could recover the IELs in these mice (Fig. 6i,j and see Supplementary Fig. 7d). Thus, these results indicate that commensal viruses and RIG-I signaling maintain IELs via APC-derived IL-15.

**Commensal viruses and RIG-I signaling promote IL-15 production via IRF-1.** Next we investigated how commensal viruses and RIG-I signaling regulated IL-15 expression. IL-15 is an NF-κB (nuclear factor κ-light-chain-enhancer of activated B cells) target gene and previous results have shown that NOD2 signaling can promote NF-κB-dependent IL-15 production to maintain IELs[16]. Moreover, RIG-I-MAVS can activate NF-κB signaling[26], so commensal viruses and RIG-I signaling might promote IL-15 production via regulation of NF-κB activation. However, we found that the APCs derived from *Ddx58*$^{-/-}$ mice had normal NF-κB-dependent cytokine production, such as tumor necrosis factor (TNF)-α and IL-6 (see Supplementary Fig. 7e,f), suggesting that other innate immune signaling pathways, such as TLR or cGAS, might compensate for the deficiency of RIG-I and the impaired IL-15 expression in *Ddx58*$^{-/-}$ APCs are not caused by the compromised NF-κB activation. In addition to NF-κB and IFN-regulatory factor (IRF)-3, RIG-I-MAVS can also activate IRF-1 activation[34]. Importantly, IRF-1 is an important transcription factor for the expression of IL-15 and can maintain IELs via promotion of its production[35,36]. Consistent with these results, we found that IL-15, but not TNF, expression in APCs was dramatically reduced in the LPLs of *Irf1*$^{-/-}$ mice (Fig. 7a,b), suggesting that commensal viruses and RIG-I signaling promote IL-15 production via IRF-1. To further confirm the specific

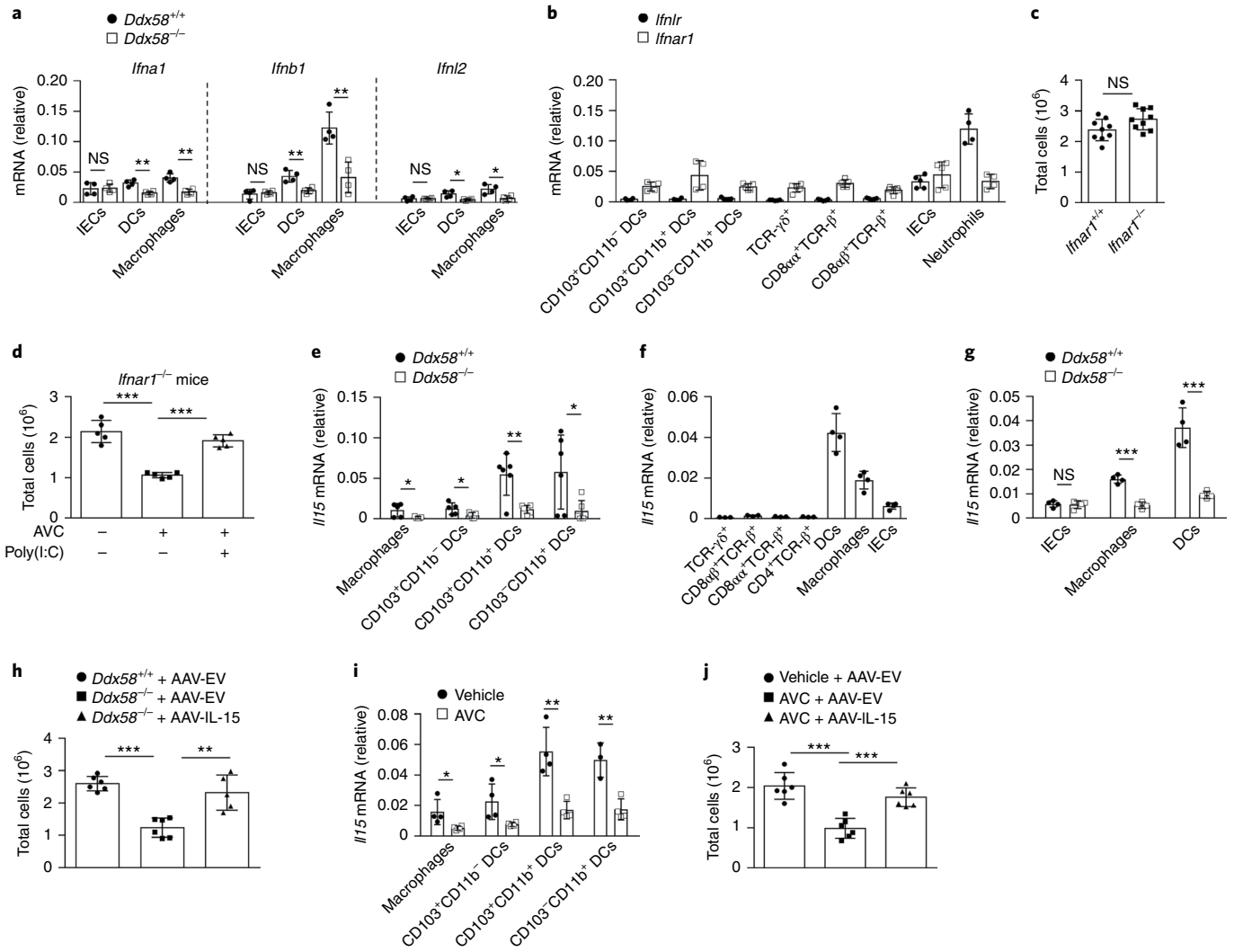


**Fig. 6 | Commensal viruses and RIG-I-MAVS signaling maintain IELs via IL-15. a**, Quantification of *Ifna1, Ifnb1* or *Ifnl2* mRNA by qPCR in the indicated cell subsets from *Ddx58*$^{+/+}$ and *Ddx58*$^{-/-}$ mice ($n=4$). **b**, Quantification of *Ifnlr* or *Ifnar1* mRNA by qPCR in the indicated cell subsets (CD103$^+$CD11b$^-$ DCs, CD103$^+$CD11b$^+$ DCs, neutrophils, $n=4$; CD103$^-$CD11b$^+$ DCs, TCR-γδ$^+$ IELs, CD8αα$^+$TCR-β$^+$ IELs, CD8αβ$^+$TCR-β$^+$ IELs, IECs, $n=5$). **c**, The number of total S-IELs from *Ifnar1*$^{-/-}$ or *Ifnar1*$^{+/+}$ mice are shown ($n=9$). **d**, The number of S-IELs in *Ifnar1*$^{-/-}$ mice treated with AVC alone or in the presence of PEI-encapsulated poly(I:C) ($n=5$). **e**, Quantification of *Il15* mRNA by qPCR in the indicated small intestinal macrophage and DC subsets (macrophages, CD103$^+$CD11b$^-$ DCs, $n=5$; CD103$^+$CD11b$^+$ DCs, CD103$^-$CD11b$^+$ DCs, $n=6$) from *Ddx58*$^{+/+}$ or *Ddx58*$^{-/-}$ mice. **f**, Quantification of *Il15* mRNA by qPCR in the indicated cell subsets (TCR-γδ$^+$ IELs, CD8αα$^+$TCR-β$^+$ IELs, CD8αβ$^+$TCR-β$^+$ IELs, CD4$^+$TCR-β$^+$ IELs, $n=3$; DCs, macrophages, IECs, $n=4$). **g**, Quantification of *Il15* mRNA by qPCR in the indicated cells from *Ddx58*$^{+/+}$ or *Ddx58*$^{-/-}$ mice ($n=4$). **h**, The number of total S-IELs from *Ddx58*$^{+/+}$ mice, *Ddx58*$^{-/-}$ mice or *Ddx58*$^{-/-}$ mice treated with AAV-expressing murine IL-15 (AAV-IL-15) ($n=6$). **i**, Quantification of *Il15* mRNA by qPCR in the indicated small intestinal macrophages and DC subsets from mice with or without AVC treatment (vehicle CD103$^-$CD11b$^+$ DCs, $n=3$; others, $n=4$). **j**, The number of S-IELs from mice treated with AVC alone or in the presence of AAV-IL-15 ($n=6$). Data pooled from three independent experiments (**c**) or two independent experiments (**a**,**b**,**d**–**j**) are shown (mean ± s.d.). The *P* values were determined using two-tailed, Student's *t*-tests (**a**,**c**,**e**,**g**,**i**) or one-way ANOVA for multiple comparisons (**d**,**h**,**j**). $^*P<0.05$, $^{**}P<0.01$, $^{***}P<0.001$.

role of IRF-1 in RIG-I signaling, activation-induced IL-15 expression, we examined the role of IRF-1 in vesicular stomatitis virus (VSV) infection or intracellular delivery of poly(I:C)-induced IL-15 expression in bone marrow DCs. The results showed that VSV- or cytosolic poly(I:C)-induced IFN-β expression was impaired in *Ddx58*$^{-/-}$ cells, but normal in *Irf1*$^{-/-}$ cells (Fig. 7c). In contrast, IL-15 expression was impaired in both *Ddx58*$^{-/-}$ and *Irf1*$^{-/-}$ cells (Fig. 7d), suggesting that IRF-1 has a specific role to regulate IL-15 expression. More importantly, similar to *Ddx58*$^{-/-}$ mice and commensally depleted mice, the CD8αα$^+$TCR-αβ$^+$ and CD8αβ$^+$TCR-αβ$^+$ IELs were decreased notably in *Irf1*$^{-/-}$ mice (Fig. 7e,f). Moreover, commensal virus depletion had no impact on the IELs in *Irf1*$^{-/-}$ mice and supplementation of poly(I:C) could rescue the IEL loss in AVC-treated *Irf1*$^{+/+}$ mice, but not in *Irf1*$^{-/-}$ mice (Fig. 7g). Although IRF-1 has been reported to regulate RIG-I expression, the intestinal APCs from *Irf1*$^{-/-}$ mice had normal *Ddx58* messenger RNA expression (Fig. 7h), suggesting that the IEL loss in *Irf1*$^{-/-}$ mice was not caused by the impaired expression of RIG-I. It should be noted that, unlike *Ddx58*$^{-/-}$ mice and commensal virus-depleted mice, TCR-γδ$^+$ IELs were also dramatically reduced in *Irf1*$^{-/-}$ mice (Fig. 7f), which is consistent with the phenotype observed in *Il15*$^{-/-}$ mice[33]. The possible reason for this is that IRF-1 deficiency not only results in the impaired expression of IL-15 in APCs, but might also be important in other types of cells, such as epithelial cells or

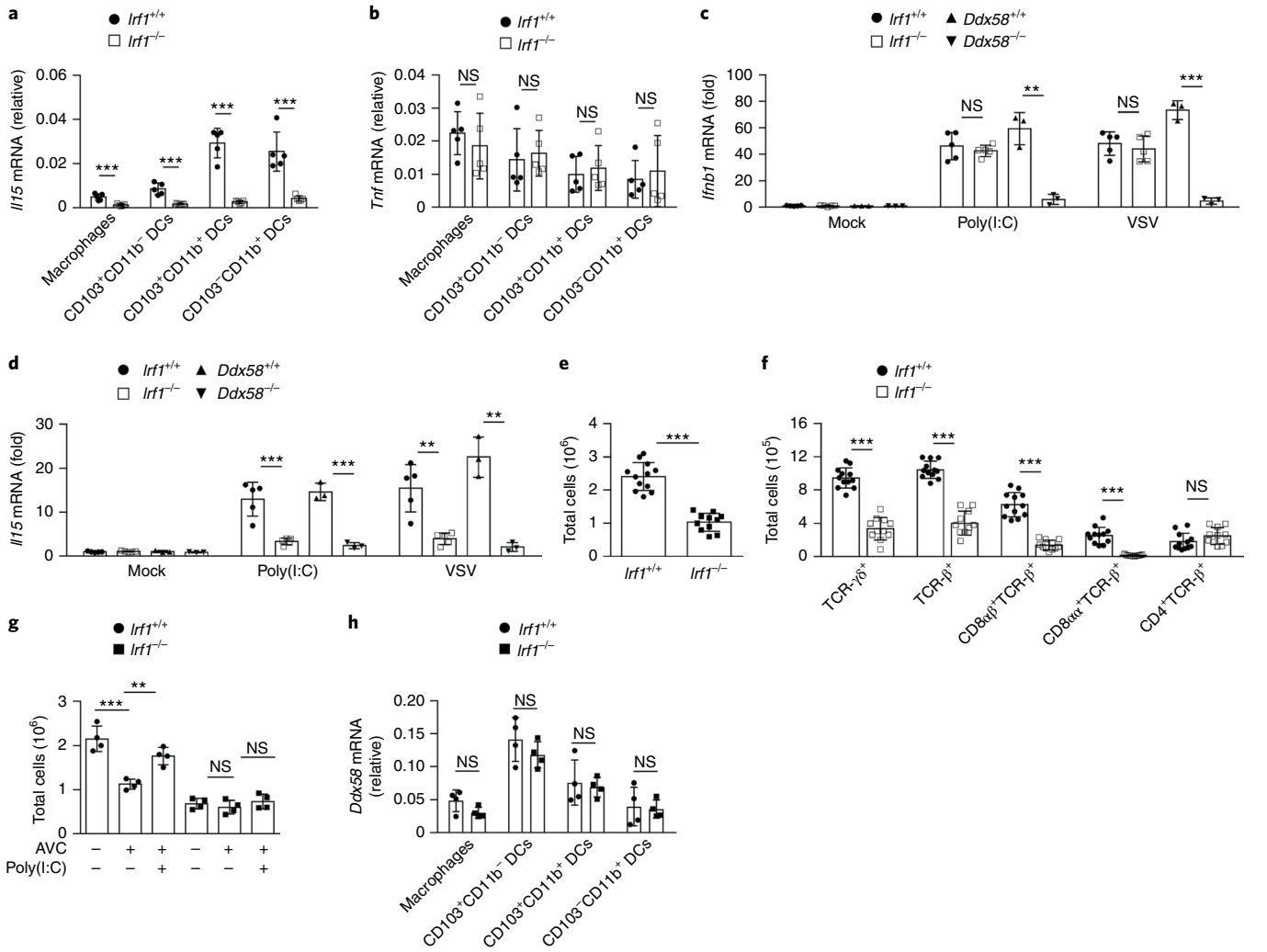


**Fig. 7 | Commensal viruses and RIG-I signaling promote IL-15 production via IRF-1. a**,**b**, Quantification of *Il15* (**a**) or *Tnf* (**b**) mRNA by qPCR in the indicated intestinal macrophage and DC subsets from *Irf1*$^{+/+}$ or *Irf1*$^{-/-}$ mice ($n=5$). The target genes were normalized to the housekeeping gene (*Gapdh*) shown as $2^{-\Delta Ct}$. **c**,**d**, Quantification of *Ifnb1* (**c**) or *Il15* (**d**) mRNA by qPCR in the bone marrow DCs from *Ddx58*$^{+/+}$ mice ($n=5$), *Ddx58*$^{-/-}$ mice ($n=5$), *Irf1*$^{+/+}$ mice ($n=3$) or *Irf1*$^{-/-}$ mice ($n=3$) that were treated with VSV or cytosolic poly(I:C). The relative gene expression level was normalized to the housekeeping gene (*Gapdh*) shown as $2^{-\Delta\Delta Ct}$. **e**,**f**, The numbers of the S-IELs (**e**) and indicated subsets (**f**) from *Irf1*$^{-/-}$ mice ($n=11$) or *Irf1*$^{+/+}$ mice ($n=12$). **g**, The number of S-IELs in *Irf1*$^{+/+}$ and *Irf1*$^{-/-}$ mice treated with AVC alone or in the presence of PEI-encapsulated poly(I:C) ($n=4$). **h**, The qPCR analysis of *Ddx58* expression in the indicated intestinal macrophages and DC subsets from *Irf1*$^{+/+}$ or *Irf1*$^{-/-}$ mice ($n=4$). Data pooled from three independent experiments (**e**,**f**) or two independent experiments (**a**–**d**,**g**,**h**) are shown (mean ± s.d.). The *P* values were determined using two-tailed, Student's *t*-tests (**a**–**h**). $^{*}P<0.05$, $^{**}P<0.01$, $^{***}P<0.001$.

fibroblasts. These results indicate that commensal viruses and RIG-I signaling maintain IELs via IRF-1.

**Recovery of IELs reverses colitis susceptibility in commensal virus-depleted mice.** IELs are located in the epithelium and have been regarded as the first line of defense against environmental challenges or pathogen invasion[12]. IELs have been reported to highly express immunoregulatory cytokines, including IL-10, TGF-β1 and TGF-β3[14,37,38], and loss of IELs in mice results in more severe colitis in several animal models and impaired host defense to bacteria[14,15,37–40], suggesting that IELs play an essential role in host defense and epithelial homeostasis. We first evaluated whether the IEL loss in AVC-treated mice could result in spontaneous inflammation or disruption of epithelial integrity. AVC treatment did not induce apparent upregulation of inflammatory cytokines or tissue damage (see Supplementary Fig. 8a,b). The intestinal permeability to fluorescein isothiocyanate (FITC)–dextran in homeostatic conditions was also not changed in AVC-treated mice (see Supplementary Fig. 8c). Similar results were also observed in *Ddx58*$^{-/-}$ mice (see Supplementary Fig. 8d–f). Both commensal virus-depleted mice and *Mavs*$^{-/-}$ mice are susceptible to dextran sulfate sodium (DSS)-induced colitis[7,8,41], so we studied whether the loss of IELs contributed to the high susceptibility of these mice to colitis. As expected, commensal virus-depleted mice showed more severe colitis during DSS treatment based on the analysis of weight loss, shortening of colon length and pathological scores (Fig. 8a–d). Moreover, when the expression of IL-15 was restored by AAV-mediated gene delivery to recover the IEL loss (Fig. 6j), the high susceptibility of commensal virus-depleted mice to DSS was reversed (Fig. 8a–d). Similarly, when the IEL loss in *Mavs*$^{-/-}$ mice was recovered by IL-15 expression (Fig. 8e), these mice showed comparable susceptibility with *Mavs*$^{+/+}$ mice (Fig. 8f–i). Thus, these results indicate that commensal viruses and RIG-I signaling can prevent tissue damage by regulating the homeostasis of IELs.

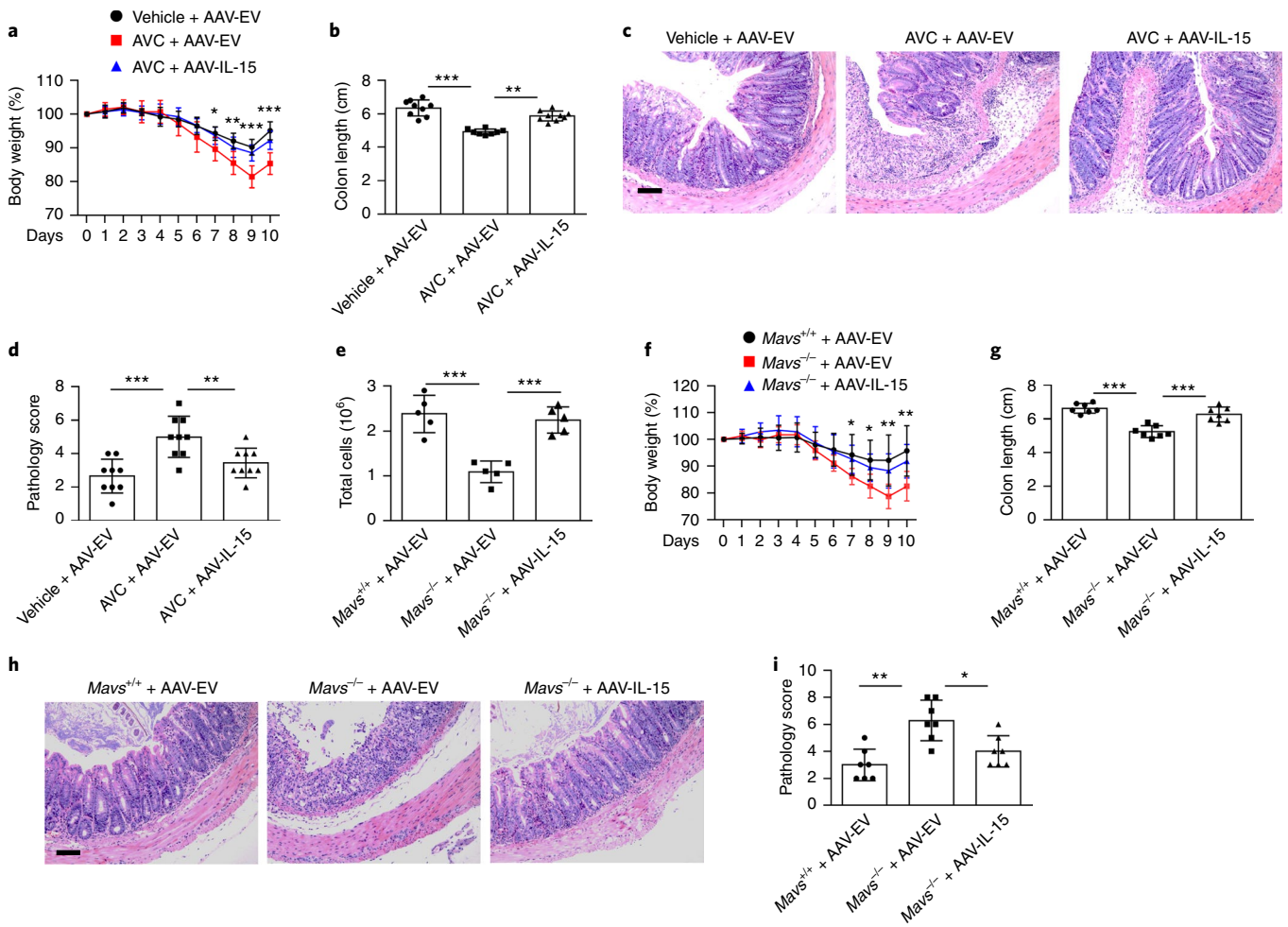


**Fig. 8 | Recovery of IELs reverses the colitis susceptibility of commensal virus-depleted mice. a**, DSS-induced body weight changes of the mice treated with AVC alone or in the presence of AAV-IL-15 ($n=9$). **b**, Colon length on day 10 (after DSS treatment) of the mice treated with AVC alone or in the presence of AAV-IL-15 ($n=9$). **c**,**d**, Representative hematoxylin and eosin staining (**c**) or quantification of pathological scores (**d**) of colon sections from the mice described in **b** ($n=9$). **e**, The number of S-IELs from *Mavs*$^{+/+}$ mice, *Mavs*$^{-/-}$ mice or *Mavs*$^{-/-}$ mice treated with AAV-IL-15 ($n=5$). **f**, DSS-induced body weight changes of *Mavs*$^{+/+}$ mice, *Mavs*$^{-/-}$ mice or *Mavs*$^{-/-}$ mice treated with AAV-IL-15 ($n=7$). **g**, Colon length on day 10 (after DSS treatment) of *Mavs*$^{+/+}$ mice, *Mavs*$^{-/-}$ mice or *Mavs*$^{-/-}$ mice treated with AAV-IL-15 ($n=7$). **h**,**i**, Representative hematoxylin and eosin staining (**h**) or quantification of pathological scores (**i**) of colon sections from the mice described in **g** ($n=7$). Scale bars: 100 μm. Data pooled from one experiment representative of at least two independent experiments (**a**–**d**,**f**–**i**) or two independent experiments (**e**) are shown (mean ± s.d.). The *P* values were determined by two-way ANOVA for multiple comparisons (**a**,**f**) or one-way ANOVA for multiple comparisons (**b**,**d**,**e**,**g**,**i**). $^{*}P<0.05$, $^{**}P<0.01$, $^{***}P<0.001$.

## Discussion

The present study demonstrates that commensal viruses are essential for the homeostasis of IELs. After recognition by RIG-I receptors expressed by intestinal APCs, commensal viruses can promote the production of IL-15 via the MAVS-IRF-1 signaling pathway to support the survival, proliferation and function of CD8αα$^{+}$TCR-αβ$^{+}$ and CD8αβ$^{+}$TCR-αβ$^{+}$ IELs. Furthermore, the loss of these IEL subsets contributes to the high susceptibility of commensal virus-depleted mice to tissue damage. Thus, our data reveal an important physiological function of commensal viruses in gut immune homeostasis.

IELs are located at the critical interface between the body and the intestinal lumen, which is exposed to microbiota, so the development and homeostasis of IELs can be shaped by microbiota. Previous studies have shown that the expansion of CD8αα$^{+}$TCR-αβ$^{+}$ and CD8αβ$^{+}$TCR-αβ$^{+}$ IELs depends on the colonization of bacteria and its products[16–18,20], suggesting the essential role of commensal bacteria in the homeostasis of IELs. Here we found that commensal virus-depleted mice have far fewer CD8αα$^{+}$TCR-αβ$^{+}$, CD8αβ$^{+}$TCR-αβ$^{+}$ and CD4$^{+}$CD8α$^{+}$TCR-αβ$^{+}$ IELs, consistent with the phenotype observed in germ-free (GF) mice[42–44], suggesting that commensal viruses might exert a similar but independent function with commensal bacteria. However, it should be noted that although our results showed that depletion of commensal viruses resulted in a minor decrease in TCR-γδ$^{+}$ IELs, GF mice have been reported to have normal TCR-γδ$^{+}$ IELs[42,44]. One possible explanation for this discrepancy is that there might be compensatory effects in GF mice to maintain TCR-γδ$^{+}$ IELs in the absence of microbiota. Indeed, dietary compounds can maintain the homeostasis of IELs as well[39]. Another possibility is that there is actually a decrease in TCR-γδ$^{+}$ IELs per centimeter of intestine in GF mice compared with SPF mice[43]; however, there is no overall difference because there is a compensatory increase in the length of the intestine in GF mice.

The commensal viruses include both eukaryotic viruses and bacteriophages[3]. Our results showed that the homeostasis of IELs depended on eukaryotic viruses, because AVC treatment caused further decrease of IELs in commensal bacteria-depleted mice. However, depletion of commensal bacteria will lead to the decrease in bacteriophages, so it is possible that the supportive role of

commensal bacteria for IELs relies on bacteriophages. Thus, the role of bacteriophages in the maintenance of IELs cannot be excluded. Indeed, the free bacteriophage particles can also be sensed by the host immune system and exert immunoregulatory roles[3]. In addition, the mammalian virome contains virus-derived retroelements in host chromosomes, which can even produce infectious particles in immunodeficient mice[3]. Moreover, it has been proposed that RIG-I recognizes endogenous retroelements[45]. However, with the consideration that AVC treatment affects only intestinal immune homeostasis and the wide distribution of retroelements, it might not be the major virome component involved in IEL homeostasis.

In this study, we showed that RIG-I could recognize commensal viruses to maintain the homeostasis of IELs. It should be noted that, although RIG-I is a sensor for viral RNA, the abundance of RNA viruses in the virome of SPF mice is very low, based on our metagenomic analysis. This raises the question of how such low-abundance RNA viruses can maintain IELs via RIG-I signaling. One possibility is that the abundance of RNA viruses in the gut virome is actually higher than we managed to identify, and many RNA viruses were not captured or characterized in our metagenomic analysis. Indeed, most of the sequencing reads could not be characterized. In addition, identifying commensal viruses, especially RNA viruses, is very challenging, and the RNA virome might be much more extensive than the currently recognized viruses because of the limitation of current technologies[3,46]. Another possibility is that DNA viruses might play a role in IEL homeostasis. Indeed, many DNA viruses can use self or host RNA polymerases to produce RNA during replication, and RIG-I has been reported to recognize DNA virus-derived RNA to induce IFNs[47]. In addition, a recent study showed that a single-stranded DNA phage produced RNA to activate host TLR-3 signaling[48], suggesting that DNA viruses might also activate RNA-sensing receptors, such as RIG-I.

Our results indicate that commensal viruses maintain IELs via an IFN-I-independent manner. Consistent with this, another report showed that conventional *Ifnar*$^{-/-}$ mice displayed normal intestinal T cells compared with WT mice[9]. However, they also showed that MNV infection restored intestinal T cells via IFN-I in commensal bacteria-depleted mice[9], suggesting that IFN-I maintains intestinal T cells during MNV infection, but not in the steady state. In addition, both this earlier study[9] and another study showed that conventional *Ifnar*$^{-/-}$ mice had comparable susceptibility to DSS compared with WT mice, although MNV infection prevented DSS-induced colitis in commensal bacteria-depleted mice in an IFN-I-dependent manner[8,9]. These results suggest that commensal viruses can maintain intestinal homeostasis and exert a beneficial role on the steady state in an IFN-I-independent manner.

Our results suggest that commensal viruses and RIG-I signaling can prevent mice from intestinal inflammation and tissue damage through maintenance of the homeostasis of IELs. Depletion of commensal viruses or MAVS deficiency rendered mice more susceptible to DSS-induced colitis, and restoration of IELs by IL-15 supplementation in these mice reduces the susceptibility to DSS. Although the detailed mechanisms of how IELs prevent tissue damage are not clear, CD8αα$^{+}$TCR-αβ$^{+}$, CD8αβ$^{+}$TCR-αβ$^{+}$ and CD4$^{+}$CD8α$^{+}$TCR-αβ$^{+}$ IELs have been reported to highly express immunoregulatory cytokines, including IL-10, TGF-β1 and TGF-β3[14,37,38], suggesting that the reduced production of these regulatory cytokines caused by IEL loss might contribute to the increased susceptibility to colitis. However, other possibilities mediated by AVC treatment that might also contribute to the increased susceptibility to colitis cannot be excluded . Indeed, commensal viruses have been reported to elicit IFN-λ to prevent DSS-induced colitis via acting on neutrophils[8]. The other effects mediated by colonization of commensal viruses need to be further investigated.

Collectively, our results demonstrate that commensal viruses and RIG-I signaling are important for the homeostasis of IELs. Considering the essential role of IELs in the epithelial homeostasis and host defense, commensal viruses might play important roles in intestinal diseases, such as inflammatory bowel disease, colon cancer and intestinal infectious diseases.

## Online content

Any methods, additional references, Nature Research reporting summaries, source data, statements of code and data availability, and associated accession codes are available at https://doi.org/10.1038/s41590-019-0513-z.

Received: 21 November 2018; Accepted: 6 September 2019;
Published online: 21 October 2019

## References

1. Honda, K. & Littman, D. R. The microbiome in infectious disease and inflammation. *Annu. Rev. Immunol.* **30**, 759–795 (2012).
2. Reyes, A. et al. Viruses in the faecal microbiota of monozygotic twins and their mothers. *Nature* **466**, 334–338 (2010).
3. Virgin, H. W. The virome in mammalian physiology and disease. *Cell* **157**, 142–150 (2014).
4. Zhang, T. et al. RNA viral community in human feces: prevalence of plant pathogenic viruses. *PLoS Biol.* **4**, e3 (2006).
5. Shi, Y. & Mu, L. An expanding stage for commensal microbes in host immune regulation. *Cell Mol. Immunol.* **14**, 339–348 (2017).
6. Lopetuso, L. R., Ianiro, G., Scaldaferri, F., Cammarota, G. & Gasbarrini, A. Gut virome and inflammatory bowel disease. *Inflamm. Bowel Dis.* **22**, 1708–1712 (2016).
7. Yang, J. Y. et al. Enteric viruses ameliorate gut inflammation via Toll-like receptor 3 and Toll-like receptor 7-mediated interferon-β production. *Immunity* **44**, 889–900 (2016).
8. Broggi, A., Tan, Y., Granucci, F. & Zanoni, I. IFN-λ suppresses intestinal inflammation by non-translational regulation of neutrophil function. *Nat. Immunol.* **18**, 1084–1093 (2017).
9. Kernbauer, E., Ding, Y. & Cadwell, K. An enteric virus can replace the beneficial function of commensal bacteria. *Nature* **516**, 94–98 (2014).
10. Cheroutre, H., Lambolez, F. & Mucida, D. The light and dark sides of intestinal intraepithelial lymphocytes. *Nat. Rev. Immunol.* **11**, 445–456 (2011).
11. Cheroutre, H. & Madakamutil, L. Acquired and natural memory T cells join forces at the mucosal front line. *Nat. Rev. Immunol.* **4**, 290–300 (2004).
12. Cheroutre, H. Starting at the beginning: new perspectives on the biology of mucosal T cells. *Annu. Rev. Immunol.* **22**, 217–246 (2004).
13. Mowat, A. M. & Agace, W. W. Regional specialization within the intestinal immune system. *Nat. Rev. Immunol.* **14**, 667–685 (2014).
14. Denning, T. L. et al. Mouse TCRαβ$^{+}$CD8αα intraepithelial lymphocytes express genes that down-regulate their antigen reactivity and suppress immune responses. *J. Immunol.* **178**, 4230–4239 (2007).
15. Olivares-Villagomez, D. et al. Thymus leukemia antigen controls intraepithelial lymphocyte function and inflammatory bowel disease. *Proc. Natl Acad. Sci. USA* **105**, 17931–17936 (2008).
16. Jiang, W. et al. Recognition of gut microbiota by NOD2 is essential for the homeostasis of intestinal intraepithelial lymphocytes. *J. Exp. Med.* **210**, 2465–2476 (2013).
17. Yu, Q. et al. MyD88-dependent signaling for IL-15 production plays an important role in maintenance of CD8αα TCRαβ and TCRγδ intestinal intraepithelial lymphocytes. *J. Immunol.* **176**, 6180–6185 (2006).
18. Qiu, Y. et al. TLR2-dependent signaling for IL-15 production is essential for the homeostasis of intestinal intraepithelial lymphocytes. *Mediators Inflamm.* **2016**, 4281865 (2016).
19. Konkel, J. E. et al. Control of the development of CD8αα$^{+}$ intestinal intraepithelial lymphocytes by TGF-β. *Nat. Immunol.* **12**, 312–319 (2011).
20. Cervantes-Barragan, L. et al. *Lactobacillus reuteri* induces gut intraepithelial CD4$^{+}$CD8αα$^{+}$ T cells. *Science* **357**, 806–810 (2017).
21. Karst, S. M., Wobus, C. E., Lay, M. & Davidson, J. Virgin HWt. STAT1-dependent innate immunity to a Norwalk-like virus. *Science* **299**, 1575–1578 (2003).
22. Ma, H., Tao, W. & Zhu, S. T lymphocytes in the intestinal mucosa: defense and tolerance. *Cell Mol. Immunol.* **16**, 216–224 (2019).
23. Ramanan, D., Tang, M. S., Bowcutt, R., Loke, P. & Cadwell, K. Bacterial sensor Nod2 prevents inflammation of the small intestine by restricting the expansion of the commensal *Bacteroides vulgatus*. *Immunity* **41**, 311–324 (2014).
24. Mueller, S. N. & Mackay, L. K. Tissue-resident memory T cells: local specialists in immune defence. *Nat. Rev. Immunol.* **16**, 79–89 (2016).
25. Cao, X. Self-regulation and cross-regulation of pattern-recognition receptor signalling in health and disease. *Nat. Rev. Immunol.* **16**, 35–50 (2016).

26. Kawai, T. & Akira, S. Innate immune recognition of viral infection. *Nat. Immunol.* **7**, 131–137 (2006).
27. Gross, M., Salame, T. M. & Jung, S. Guardians of the gut—murine intestinal macrophages and dendritic cells. *Front Immunol.* **6**, 254 (2015).
28. Zhu, H. et al. RNA virus receptor Rig-I monitors gut microbiota and inhibits colitis-associated colorectal cancer. *J. Exp. Clin. Cancer Res.* **36**, 2 (2017).
29. Cheroutre, H. & Lambolez, F. The thymus chapter in the life of gut-specific intraepithelial lymphocytes. *Curr. Opin. Immunol.* **20**, 185–191 (2008).
30. Gangadharan, D. et al. Identification of pre- and postselection TCRαβ$^+$ intraepithelial lymphocyte precursors in the thymus. *Immunity* **25**, 631–641 (2006).
31. Fischer, J. C. et al. RIG-I/MAVS and STING signaling promote gut integrity during irradiation- and immune-mediated tissue injury. *Sci. Transl. Med.* **9**, eaag2513 (2017).
32. Fujihashi, K., McGhee, J. R., Yamamoto, M., Peschon, J. J. & Kiyono, H. An interleukin-7 internet for intestinal intraepithelial T cell development: knockout of ligand or receptor reveal differences in the immunodeficient state. *Eur. J. Immunol.* **27**, 2133–2138 (1997).
33. Cao, X. et al. Defective lymphoid development in mice lacking expression of the common cytokine receptor γ chain. *Immunity* **2**, 223–238 (1995).
34. Odendall, C. et al. Diverse intracellular pathogens activate type III interferon expression from peroxisomes. *Nat. Immunol.* **15**, 717–726 (2014).
35. Ohteki, T. et al. The transcription factor interferon regulatory factor 1 (IRF-1) is important during the maturation of natural killer 1.1 $^+$T cell receptor-α/β$^+$ (NK1$^+$ T) cells, natural killer cells, and intestinal intraepithelial T cells. *J. Exp. Med.* **187**, 967–972 (1998).
36. Ogasawara, K. et al. Requirement for IRF-1 in the microenvironment supporting development of natural killer cells. *Nature* **391**, 700–703 (1998).
37. Kamanaka, M. et al. Expression of interleukin-10 in intestinal lymphocytes detected by an interleukin-10 reporter knockin tiger mouse. *Immunity* **25**, 941–952 (2006).
38. Das, G. et al. An important regulatory role for CD4$^+$CD8αα T cells in the intestinal epithelial layer in the prevention of inflammatory bowel disease. *Proc. Natl Acad. Sci. USA* **100**, 5324–5329 (2003).
39. Li, Y. et al. Exogenous stimuli maintain intraepithelial lymphocytes via aryl hydrocarbon receptor activation. *Cell* **147**, 629–640 (2011).
40. Luda, K. M. et al. IRF8 Transcription-factor-dependent classical dendritic cells are essential for intestinal T cell homeostasis. *Immunity* **44**, 860–874 (2016).
41. Li, X. D. et al. Mitochondrial antiviral signaling protein (MAVS) monitors commensal bacteria and induces an immune response that prevents experimental colitis. *Proc. Natl Acad. Sci. USA* **108**, 17390–17395 (2011).
42. Bandeira, A. et al. Localization of γ/δ T cells to the intestinal epithelium is independent of normal microbial colonization. *J. Exp. Med.* **172**, 239–244 (1990).
43. Hoytema van Konijnenburg, D. P. et al. Intestinal epithelial and intraepithelial T cell crosstalk mediates a dynamic response to infection. *Cell* **171**, 783–794 e713 (2017).
44. Sujino, T. et al. Tissue adaptation of regulatory and intraepithelial CD4$^+$ T cells controls gut inflammation. *Science* **352**, 1581–1586 (2016).
45. Zeng, M. et al. MAVS, cGAS, and endogenous retroviruses in T-independent B cell responses. *Science* **346**, 1486–1492 (2014).
46. Manso, C. F., Bibby, D. F. & Mbisa, J. L. Efficient and unbiased metagenomic recovery of RNA virus genomes from human plasma samples. *Sci. Rep.* **7**, 4173 (2017).
47. Chiu, Y. H., Macmillan, J. B. & Chen, Z. J. RNA polymerase III detects cytosolic DNA and induces type I interferons through the RIG-I pathway. *Cell* **138**, 576–591 (2009).
48. Sweere, J. M. et al. Bacteriophage trigger antiviral immunity and prevent clearance of bacterial infection. *Science* **363**, eaat9691 (2019).


## Acknowledgements

We thank S. Akria, J. Tschopp, M. Colonna, Z. Yi and Z. Jiang for providing mice lines. We thank T. Xue for providing AAV plasmids. This work was supported by the National Key R&D program of China (grant no. 2018YFA0507403 to R.Z.), the Strategic Priority Research Program of the Chinese Academy of Sciences (grant no. XDB29030102 to R.Z. and S.Z.), the National Natural Science Foundation of China (grant nos. 31770991 to W.J., 91742202 to R.Z., 81525013 to R.Z., 81722022 to W.J., 81821001 to R.Z., W.J. and S.Z., 81788101 to R.Z.) and the Young Talent Support Program and the Fundamental Research Funds for the Central Universities.

## Author contributions

L.L., T.G., W.T., B.L., X.Z. and C.L. performed the experiments for this work. L.L., S.Z., W.J. and R.Z. designed the research. L.L., T.G., W.J. and R.Z. wrote the manuscript. W.J. and R.Z. supervised the project.

## Competing interests

The authors declare no competing interests.

## Additional information

**Extended data** is available for this paper at https://doi.org/10.1038/s41590-019-0513-z.

**Supplementary information** is available for this paper at https://doi.org/10.1038/s41590-019-0513-z.

**Correspondence and requests for materials** should be addressed to S.Z., W.J. or R.Z.

**Peer review information** Zoltan Fehervari was the primary editor on this article and managed its editorial process and peer review in collaboration with the rest of the editorial team.

**Reprints and permissions information** is available at www.nature.com/reprints.

**Publisher's note** Springer Nature remains neutral with regard to jurisdictional claims in published maps and institutional affiliations.

## Methods

**Mice.** *Ddx58*$^{-/-}$ (ref. [49]) and *Trif*$^{-/-}$ (ref. [50]) mice were provided by Dr. Shizuo Akira (Osaka University). *Ddx58*$^{-/-}$ mice were backcrossed 10 generations to BALB/C background before the experiments. *Mavs*$^{-/-}$ (ref. [51]) mice were provided by J. Tschopp (University of Lausanne). *Mda5*$^{-/-}$(ref. [52]) mice were provided by M. Colonna (Washington University). *Tmem173*$^{-/-}$ mice were provided by Z. Jiang (Peking University). *Cd11c-cre*, *Villin-cre*, *Ifnar*$^{-/-}$ and *Irf1*$^{-/-}$ mice were purchased from the Jackson laboratory. TCR-δ–GFP mice were provided by Z. Yi (Jinan University). C57BL/6J mice and *Rag2*$^{-/-}$ mice on a BALB/C background were purchased from Model Animal Research Center. *Ddx58*$^{fl/fl}$ mice were generated by Cyagen Company. Mouse genomic fragments containing homology arms and conditional knockout region were amplified from the BAC clone by using high-fidelity Taq, and were sequentially assembled into a targeting vector together with recombination sites and selection markers (see Supplementary Fig. 5a). The linearized vector was subsequently delivered to embryonic stem (ES) cells (C57BL/6J) via electroporation, followed by drug selection, PCR screening and Southern blot confirmation. Then ES cells were microinjected into C57BL/6J blastocysts. Chimeric offspring were backcrossed to C57BL/6J mice, and germline transmission was confirmed by PCR of tail genomic DNA. Founders were confirmed as germline transmitted via crossbreeding with Flp-deleter. Primers for genotyping of the *Ddx58*$^{fl/fl}$ allele were as follows: F1: AGGCCCAAGGATAATTGAAACCC; R1: CTGCCTGGCATCACATCACTAGTT. The use of primers produced bands of 289 base pair for the WT allele and 417 base pair for the *Ddx58*$^{fl/fl}$ Neo-deleted allele. The littermates of the mutant mice were used as the control in the present study except for co-housing experiments. For co-housing experiments, *Ddx58*$^{-/-}$ and their littermate WT mice originating from the same breeders were separated for two generations. After that, *Ddx58*$^{-/-}$ mice were co-housed with sex- and aged-matched WT mice for 4 weeks (co-housing) or still housed separately (single housing). Unless indicated, the mutant mice and their littermate controls used in the present study were housed separately. Mice were SPF, maintained under a strict 12 h light cycle (lights on at 07:00 and off at 19:00). All animal experiments were approved by the Ethics Committee of University of Science and Technology of China.

**Cell preparation.** IELs were isolated as previously described[16]. In brief, the small intestine or colon was opened longitudinally and cut into 1-cm-long pieces after removing PPs. The specimens were washed twice in phosphate-buffered saline (PBS) containing 100 U ml$^{-1}$ of penicillin and 100 μg ml$^{-1}$ of streptomycin, and then stirred at 37 °C in 1× Hank's containing 100 U ml$^{-1}$ of penicillin, 100 μg ml$^{-1}$ of streptomycin and 5% fetal calf serum (FCS) for 30 min. The supernatants were then separated by a 40–70% Percoll density gradient (GE Healthcare), and the cells that layered between the 40% and 70% fractions were collected as IELs. For LPL isolation, the tissues were shaking in 1× Hank's buffer containing 2 mM ethylenediaminetetraacetic acid at 37 °C for 30 min after IEL isolation. This step was repeated and the supernatants were discarded. The tissues were then digested in 1× Hank's buffer supplemented with 0.5 mg ml$^{-1}$ of collagenase IV (Sigma Aldrich) and 10% FCS at 37 °C for 20 min. After that, tissues were vortexed vigorously and the suspension was filtered using a 70-mm cell strainer. Released cells were then washed in PBS containing 5% FCS and subjected to Percoll fractionation as described above for the isolation of IELs. For IEC isolation, the small intestines were opened longitudinally and cut into 1-cm-long pieces. The specimens were washed twice in PBS containing 100 U ml$^{-1}$ of penicillin and 100 μg ml$^{-1}$ of streptomycin, and then stirred at 37 °C in 1× Hank's buffer containing 100 U ml$^{-1}$ of penicillin, 100 μg ml$^{-1}$ of streptomycin and 5% FCS for 30 min. The suspension was filtered with 70-mm cell strainer and the CD45$^{-}$EpCAM$^{+}$ IECs were sorted by FACSAria flow cytometer (BD). For isolation of liver lymphocytes, the murine liver was removed and cut into small pieces, and passed through 70-mm cell strainer. After a 5-min incubation at 4 °C, the cells were pelleted and subjected to Percoll fractionation as described above for the isolation of IELs. For thymocyte and splenocyte isolation, the organs were directly grinded and suspended in 5 ml PBS containing 5% FBS. For analysis of MLNs and PPs, the organs were cut into small pieces and enzymatically digested with Collagenase IV (0.5 mg ml$^{-1}$, Sigma Aldrich) at 37 °C for 20 min and then filtered before analysis.

**Flow cytometry analysis.** Suspensions of lymphocytes were stained with mouse monoclonal antibodies and immunoglobulin Gs were used as negative control. All antibodies were purchased from Thermo Fisher Scientific or BD. The following monoclonal antibody conjugates were used: TCR-γδ–FITC and –PE (GL3); TCR-β–FITC and –PE-Cy5.5 (H57-597); CD4–FITC, –PE-Cy7 and –allophycocyanin–eFluor780 (GK1.5); CD8α–allophycocyanin–eFluor780, –allophycocyanin and –PE-Cy7 (53-6.7); CD8β–PE, –PE–Cy7 and –FITC (H35-17.2); CD19–FITC(1D3); CD3ε–FITC (145-2C11); B220–PE–Cy7 (RA3-6B2); CD11C–PE–Cy7 (HL3); CD11b–PE–CY5.5 (M1/70); CD49b–FITC (DX5); major histocompatibility complex (MHC)-II–allophycocyanin–eFluor780 (M5/114.15.2); CD64–PE (X54-5/7.1); CD45–allophycocyanin–eFluor780 and –PE (30-F11); CD62L–FITC (MEL-14); CD122–PE; CD44–allophycocyanin–eFluor780(IM7); NK1.1–PE–CY7 (PK136); CD103–allophycocyanin (2E7); and FITC–EpCAM(G8.8). BD Verse cytometers were used for flow cytometry and FlowJo v.10.0.7 was used to analyze the data. A FACSAria flow cytometer (BD) was used for cell sorting and purification.

**Cell stimulation.** For inducing IL-15 or IFN-β, 1.5 × 10$^{6}$ bone marrow DCs were plated in six-well plates overnight, and the medium was changed to Opti-MEM the next morning. After that, the cells were stimulated with VSV (multiplicity of infection = 1) for 7 h. For cytosol delivery, low-molecular-weight poly(I:C) (4 μg ml$^{-1}$) was transfected using Lipofectamine 2000 according to the manufacturer's protocol (Thermo Fisher Scientific).

**MNV analysis.** The in vivo MNV analysis was performed as previously described[53]. In brief, mice were orally given a dose of 10$^{6}$ plaque-forming units of the MNV-1. After 24 h, the stool was collected from MNV-infected or noninfected mice and stored at −80 °C. RNA from stool was isolated with an Allperp Power DNA/RNA kit (Qiagen) and complementary DNA was synthesized with an M-MLV Reverse Transcriptase kit according to the manufacturer's protocol (Thermo Fisher Scientific). The PCR primers used are: MNV—forward: AGGTCATGCGAGATC AGCTT; MNV—reverse: CCAAGCTCTCACAAGCCTTC.

**Commensal virus/bacteria depletion and RIG-I ligand reconstitution.** The commensal virus was depleted with an antiviral cocktail as previously described[7,8]. In brief, 2-week-old mice were orally given an antiviral cocktail containing ribavirin (30 mg kg$^{-1}$; Selleck), lamivudine (10 mg kg$^{-1}$; Selleck) and aciclovir (20 mg kg$^{-1}$; Selleck) once a day for 6 weeks. For RIG-I ligand reconstitution, mice were intraperitoneally injected with PEI-encapsulated, low-molecular-weight poly(I:C) (20 μg per mouse; Invivogen) or poly(A:T) (20 μg per mouse; Invivogen) once a day for 2 weeks before experiments. For commensal bacteria depletion, 2-week-old mice were given drinking water containing vancomycin (0.5 g l$^{-1}$; Biosharp), neomycin (1 g l$^{-1}$; Biosharp), ampicillin (1 g l$^{-1}$; Biosharp) and metronidazole (1 g l$^{-1}$; Biosharp) for 6 weeks according to the methods previously described[54].

**Qualification of fecal VLPs.** The virus-like particles (VLPs) of feces were determined as previously described[55]. In brief, 0.1 g fresh feces was collected and then suspended in 2 ml filtered, sterilized SM buffer (8 mM $MgSO_4$, 100 mM NaCl, 50 mM Tris-HCl, pH 7.4, and 0.002%, w/v, gelatin). The samples were subsequently centrifuged at 2,500*g* for 10 min at 4 °C and then filtered with 0.45-μm (Millex-HV) and 0.22–μm filters (Millipore) to remove cell debris and bacteria. The VLPs of AVC-treated or -untreated samples were serially diluted and compared in the same dilution. Filtrates were filtered on to a 0.02-μm Anodisc polycarbonate filter (Whatman). Filters with viral particles were stained with 10× SYBR Gold (Thermo Fisher Scientific) and 10× SYBR Green II (Thermo Fisher Scientific) for 15 min, respectively. After that, the filters were washed once and imaged at a ×40 magnification. Stained particles <0.5 μm in diameter were regarded as VLPs. SM buffer was used as a negative control.

**Metagenomic sequencing of VLPs.** Fecal VLP particles were purified according to previously described method[55]. Briefly, fresh feces (1 g) from C57BL/6J mice were suspended in 5 ml filtered, sterilized SM buffer, then subsequently centrifuged at 2,500*g* for 10 min at 4 °C, and filtered with 0.45-μm (Millex-HV) and 0.22-μm filters (Millipore) to remove cell debris and bacteria. The suspension was transferred into a 100-kDa Ultrafiltration centrifuge (Millipore) and centrifuged at 4,500*g* for 20 min to concentrate VLPs. Then the suspension was treated with DNase I (Ambion) at 37 °C for 1 h to remove capsid-free DNA before use for viral DNA or RNA extraction by Allperp Power DNA/RNA kit (Qiagen). The VLP-derived DNA was amplified using a multiple displacement amplification protocol by REPLI-g Single Cell Kit (Qiagen), according to the manufacturer's instructions. For the viral RNA amplification, the extracted DNA/RNA was initially treated with DNase I at 37 °C for 1 h and then amplified using a random-primer protocol as previously described[56]. The amplified DNA was used as input for the NEBNext Ultra II DNA Library Prep kit to construct a next-generation sequencing library, and then sequenced on an Illumina HiSeq sequencing 4000 system (Illumina) using 150/150-base pair paired-end sequencing. Raw data were first cleaned by trimming adapters and removing low-quality sequences, and then taxonomically classified by Kraken[57,58]. Reads assigned to a viral taxon were kept for the following analysis.

**16S ribosomal RNA bacterial community analysis.** Metagenomic DNA extraction from feces was performed using QIAamp PowerFecal DNA Kit (Qiagen). According to the results of sample pre-amplification, appropriate DNA metagenomic DNA was used for PCR reaction with V4 primers and PCR master mix. The PCR products were purified using a QIAquick PCR Purification Kit (Qiagen) and were then incubated with End Repair Mix at 20 °C for 30 min. The end-repaired DNA was purified using a QIAquick PCR Purification Kit and then incubated with A-Tailing Mix at 37 °C for 30 min. The purified adenylate 3′-end DNA was incubated with adapter and ligation mix at 16 °C for 12–16 h. Adapter-ligated DNA was selected by running a 2.5% agarose gel for about 2.5–3 h to recover the target fragments. The DNA was purified from the gel using the QIAquick Gel Extraction kit (Qiagen) to validate the libraries. The qualified libraries were amplified on cBot to generate the cluster on the flow cell (TruSeq PE Cluster Kit V3-cB-HS, Illumina). The amplified flow cell was sequenced pair-end on the HiSeq 2000 System (TruSeq SBS KIT-HS V3, Illumina). The operational taxonomic units were based on 97% sequences similarity to the Greengenes

13_5 database. The richness (number of observed species) and alpha diversities (Shannon index) were calculated in QIIME.

**In vivo permeability assay.** For in vivo permeability assay, the mice were kept without water overnight and then were orally administered water containing FITC–dextran (500 mg kg$^{-1}$; Sigma Aldrich). After 4 h, the plasma was collected and diluted twofold in PBS, and the fluorescence was determined at 528 nm with excitation at 485 nm using a plate reader (BioTek).

**Cell proliferation and apoptosis analysis.** Apoptosis assay was performed as previously described[16]. In brief, IELs were initially labeled with the appropriate monoclonal antibody. After washing, cells were stained with an annexin-V staining kit (MultiSciences) according to the manufacturer's protocol, and were then analyzed on BD Verse cytometers. For cell proliferation assay, mice were injected intraperitoneally with 1.8 mg BrdU (Sigma Aldrich) diluted in PBS. After that, mice were given drinking water containing 0.8 mg ml$^{-1}$ of BrdU and 5% glucose. Water containing BrdU was changed every 3 d. After 10 d, mice were sacrificed and the IELs were stained with a BrdU staining kit (BD Pharmingen) according to the manufacturer's protocol.

**Adoptive transfers.** For BM chimera experiments, *Ddx58*$^{+/+}$ or *Ddx58*$^{-/-}$ BM cells were intravenously transferred into irradiated *Rag2*$^{-/-}$ mice (3 Gy), or *Ddx58*$^{+/+}$ BM cells were intravenously transferred into lethally irradiated (10 Gy given 1 d before adoptive transfer) *Ddx58*$^{+/+}$ or *Ddx58*$^{-/-}$ mice, or *Ddx58*$^{-/-}$ BM cells were intravenously transferred into lethally irradiated *Ddx58*$^{+/+}$ or *Ddx58*$^{-/-}$ mice. After 8 weeks, IELs were analyzed by flow cytometry.

**Real-time PCR.** For cells and tissues, total RNA was extracted with TRIzol reagent (Thermo Fisher Scientific) in accordance with the manufacturer's instructions and complementary DNA was synthesized with an M-MLV Reverse Transcriptase kit according to the manufacturer's protocol (Thermo Fisher Scientific). Real-time PCR was performed using SYBR Green master mix (TransGen) by a Step One Real Time PCR System (Applied Biosystems). The target genes were normalized to the housekeeping gene (*Gapdh*) shown as $2^{-\Delta Ct}$. The used primers are as follows:

*Il15*—forward: 5′-ATTCTCTGCGCCCAAAAGAC-3′
*Il15*—reverse: 5′-GTGGATTCTTTCCTGACCTCT-3′
*Tnf*—forward: 5′-CATCTTCTCAAAATTCGAGTGACAA-3′
*Tnf*—reverse: 5′-TGGGAGTAGACAAGGTACAACCC-3′
*Gapdh*—forward: 5′-GGTGAAGGTCGGTGTGAACG-3′
*Gapdh*—reverse: 5′-CTCGCTCCTGGAAGATGGTG-3′
*Tgfβ1*—forward: 5′-ACGTCACTGGAGTTGTACGG-3′
*Tgfβ1*—reverse: 5′-GGGCTGATCCCGTTGATTTC-3′
*Ifnar1*—forward: 5′-GGTCATTACTGTCACCGCCA-3′
*Ifnar1*—reverse: 5′-ACACAGTACACAGTCAGCGG-3′
*Ifnlr*—forward: 5′-CCCAGCAACTCCTAAGCCAA-3′
*Ifnlr*—reverse 5′-TGCCCTGAACCAACCAATGT-3′
*Il6*—forward: 5′-GAGGATACCACTCCCAACAGACC-3′
*Il6*—reverse: 5′-AAGTGCATCATCGTTGTTCATACA-3′
*Ifnl2*—forward: 5′-GCAGTTCCCACCTCATCTCC-3′
*Ifnl2*—reverse: 5′-CTGTGGCCTGAAGCTGTGTA-3′
*Ifna1*—forward: 5′-CTACTGGCCAACCTGCTCTC-3′
*Ifna1*—reverse: 5′-CCTTCTTGATCTGCTGGGCA-3′
*Ifnb1*—forward: 5′-CCAGCTCCAAGAAAG GACGA-3′
*Ifnb1*—reverse: 5′-GGAGCATCTCTTGGATGGCA-3′
*Il10*—forward: 5′-GGTTGCCAAGCCTTATCGGA-3′
*Il10*—reverse: 5′-AATCGATGACAGCGCCTCAG-3′
*Il12p40*—forward: 5′-TGGTTTGCCATCGTTTTGCTG-3′
*Il12p40*—reverse: 5′-ACAGGTGAGGTTCACTGTTTCT-3′
*Ifng*—forward: 5′-AGGAACTGGCAAAAGGATGGT-3′
*Ifng*—reverse: 5′-ACCTGTGGGTTGTTGACCTC-3′
*Il7*—forward: 5′-CCTCCACTGATCCTTGTTCTG-3′
*Il7*—reverse: 5′-TGCGAGCAGCACGATTTAG-3′

**AAV-mediated *Il15* gene delivery.** The sequence encoding mouse *Il15* was cloned into the plasmid pscAAV-GFP and then recombined with the pHelper plasmid to produce the recombinant plasmid AAV–IL-15. AAV–IL-15 or empty vector was transfected into HEK-293T cells (the cells were from American Type Culture Collection and were not authenticated in our lab, but were routinely tested for mycoplasma contamination) to generate AAV particles. After titration, $2 \times 10^9$ virus particles were injected intravenously into mice. After 2 weeks, the mice were used for the experiments.

**Induction of DSS colitis.** To induce colitis, mice were given 2.5% (w/v) DSS (MP Biomedicals) in the drinking water for 7 d, and then switched to regular drinking water for 2 d. Mice were weighed every day to determine percentage weight changes and calculated as percentage body weight change. Mice were killed on day 10 and the length of colon was determined.

**Immunohistochemistry and immunofluorescence.** The small intestine and colon tissue were fixed in 10% neutral-buffered formalin and embedded in paraffin; 5-μm sections were affixed to slides, and then deparaffinized and stained with CD8α antibodies (Cell Signaling Technology). The number of positive staining cells were counted under a light microscope (DP72; Olympus). For TCR-γδ IEL analysis, TCR-δ–GFP mice were fed an AVC cocktail as previous described and then sacrificed. Frozen sections of the small intestine and colon tissue were mounted with ProLong Gold reagent DAPI (Thermo Fisher Scientific, Invitrogen). Images were obtained using a fluorescence microscope (DP72; Olympus).

**Hematoxylin and eosin staining.** For histology, colon tissue was fixed in 10% neutral-buffered formalin and embedded in paraffin; 5-μm sections were affixed to slides, deparaffinized and stained with hematoxylin and eosin. Morphological changes in the stained sections were examined under a light microscope (BX53, Olympus). The histological scores were measured as previously described[59]. In brief, the histological scores includes severity of inflammation (0—none; 1—slight; 2—moderate; 3—severe), extent of injury (0—none; 1—mucosal; 2—mucosal and submucosal; 3—transmucosal) and crypt damage (0—none; 1—basal one-third damaged; 2—basal two-thirds damaged; 3—only surface epithelium intact; 4—entire crypt and epithelium lost).

**Statistical analysis.** All values are expressed as the mean ± s.d. Statistical analysis was performed using unpaired, Student's *t*-tests for two groups and one-way analysis of variance (ANOVA) or two-way ANOVA (GraphPad Software) for multiple groups, with all data points showing a normal distribution. The researchers were not blinded to the distribution of treatment groups when performing experiments and data assessment. Sample sizes were selected on the basis of preliminary results to ensure an adequate power. $P < 0.05$ was considered significant.

**Reporting Summary.** Further information on research design is available in the Nature Research Reporting Summary linked to this article.

## Data availability

The EMBL-EBL accession number for viral metagenomics sequences and the 16S ribosomal RNA bacterial sequences is PRJEB27933. The data that support the other findings of this study are available from the corresponding author upon reasonable request.

## References


49. Kato, H. et al. Cell type-specific involvement of RIG-I in antiviral response. *Immunity* **23**, 19–28 (2005).
50. Yamamoto, M. et al. Role of adaptor TRIF in the MyD88-independent toll-like receptor signaling pathway. *Science* **301**, 640–643 (2003).
51. Michallet, M. C. et al. TRADD protein is an essential component of the RIG-like helicase antiviral pathway. *Immunity* **28**, 651–661 (2008).
52. Gitlin, L. et al. Essential role of mda-5 in type I IFN responses to polyriboino sinic:polyribocytidylic acid and encephalomyocarditis picornavirus. *Proc. Natl Acad. Sci. USA* **103**, 8459–8464 (2006).
53. Baldridge, M. T. et al. Commensal microbes and interferon-λ determine persistence of enteric murine norovirus infection. *Science* **347**, 266–269 (2015).
54. Rakoff-Nahoum, S., Paglino, J., Eslami-Varzaneh, F., Edberg, S. & Medzhitov, R. Recognition of commensal microflora by toll-like receptors is required for intestinal homeostasis. *Cell* **118**, 229–241 (2004).
55. Thurber, R. V., Haynes, M., Breitbart, M., Wegley, L. & Rohwer, F. Laboratory procedures to generate viral metagenomes. *Nat. Protoc.* **4**, 470–483 (2009).
56. Wang, D. et al. Microarray-based detection and genotyping of viral pathogens. *Proc. Natl Acad. Sci. USA* **99**, 15687–15692 (2002).
57. Wood, D. E. & Salzberg, S. L. Kraken: ultrafast metagenomic sequence classification using exact alignments. *Genome Biol.* **15**, R46 (2014).
58. Menzel, P., Ng, K. L. & Krogh, A. Fast and sensitive taxonomic classification for metagenomics with Kaiju. *Nat. Commun.* **7**, 11257 (2016).
59. Dieleman, L. A. et al. Chronic experimental colitis induced by dextran sulphate sodium (DSS) is characterized by Th1 and Th2 cytokines. *Clin. Exp. Immunol.* **114**, 385–391 (1998).

nature research

Corresponding author(s): Rongbin Zhou, Wei Jiang, Shu Zhu

Last updated by author(s): Aug 31, 2019

# Reporting Summary

Nature Research wishes to improve the reproducibility of the work that we publish. This form provides structure for consistency and transparency in reporting. For further information on Nature Research policies, see Authors & Referees and the Editorial Policy Checklist.

## Statistics

For all statistical analyses, confirm that the following items are present in the figure legend, table legend, main text, or Methods section.

| n/a | Confirmed | |
|---|---|---|
| ☐ | ☒ | The exact sample size (*n*) for each experimental group/condition, given as a discrete number and unit of measurement |
| ☐ | ☒ | A statement on whether measurements were taken from distinct samples or whether the same sample was measured repeatedly |
| ☐ | ☒ | The statistical test(s) used AND whether they are one- or two-sided<br>*Only common tests should be described solely by name; describe more complex techniques in the Methods section.* |
| ☒ | ☐ | A description of all covariates tested |
| ☐ | ☒ | A description of any assumptions or corrections, such as tests of normality and adjustment for multiple comparisons |
| ☐ | ☒ | A full description of the statistical parameters including central tendency (e.g. means) or other basic estimates (e.g. regression coefficient) AND variation (e.g. standard deviation) or associated estimates of uncertainty (e.g. confidence intervals) |
| ☐ | ☒ | For null hypothesis testing, the test statistic (e.g. *F*, *t*, *r*) with confidence intervals, effect sizes, degrees of freedom and *P* value noted<br>*Give P values as exact values whenever suitable.* |
| ☒ | ☐ | For Bayesian analysis, information on the choice of priors and Markov chain Monte Carlo settings |
| ☒ | ☐ | For hierarchical and complex designs, identification of the appropriate level for tests and full reporting of outcomes |
| ☒ | ☐ | Estimates of effect sizes (e.g. Cohen's *d*, Pearson's *r*), indicating how they were calculated |

*Our web collection on statistics for biologists contains articles on many of the points above.*

## Software and code

Policy information about availability of computer code

| | |
|---|---|
| Data collection | BD Verse cytometers, BD FACSAria flow cytometer , Illumina HiSeq 2000 System, Illumina HiSeq sequencing 4000 system, a Step One Real Time PCR System (Applied Biosystems), DP72(Olympus), BioTek Synergy2, Bio-Rad ChemiDoc XRS+. |
| Data analysis | Stastical analysis is used to GraphPad Software(6.0). Flowjo(v10.0.7) for FACS data analysis is used. Western blot is analyzed by Image Lab. Principal Component Analysis (PCA) was performed by R Version v3.1.1. Community diversity and taxonomy were analyzed by Qiime 1.9.1. Images were obtained using a Fluorescence or light microscopy(DP72; Olympus). |

For manuscripts utilizing custom algorithms or software that are central to the research but not yet described in published literature, software must be made available to editors/reviewers. We strongly encourage code deposition in a community repository (e.g. GitHub). See the Nature Research guidelines for submitting code & software for further information.

## Data

Policy information about availability of data

All manuscripts must include a data availability statement. This statement should provide the following information, where applicable:

- Accession codes, unique identifiers, or web links for publicly available datasets
- A list of figures that have associated raw data
- A description of any restrictions on data availability

The EMBL-EBL accession number for viral metagenomics sequences and the 16S rRNA Bacterial sequences are PRJEB27933. The data that support the other findings of this study are available from the corresponding author upon reasonable request.

# Field-specific reporting

Please select the one below that is the best fit for your research. If you are not sure, read the appropriate sections before making your selection.

☒ Life sciences ☐ Behavioural & social sciences ☐ Ecological, evolutionary & environmental sciences

For a reference copy of the document with all sections, see nature.com/documents/nr-reporting-summary-flat.pdf

# Life sciences study design

All studies must disclose on these points even when the disclosure is negative.

| | |
|---|---|
| Sample size | Sample sizes were selected on the basis of preliminary results to ensure an adequate power. |
| Data exclusions | No data was excluded. |
| Replication | all experiments were repeated at least twice. The exact repeat times were provided in figure legends. |
| Randomization | No randomization was used. Animals used for experiments were age and sex matched. |
| Blinding | The researchers were not blinded to the distribution of treatment groups when performing experiments and data assessment. |

# Reporting for specific materials, systems and methods

We require information from authors about some types of materials, experimental systems and methods used in many studies. Here, indicate whether each material, system or method listed is relevant to your study. If you are not sure if a list item applies to your research, read the appropriate section before selecting a response.

## Materials & experimental systems

| n/a | Involved in the study |
|---|---|
| ☐ | ☒ Antibodies |
| ☐ | ☒ Eukaryotic cell lines |
| ☒ | ☐ Palaeontology |
| ☐ | ☒ Animals and other organisms |
| ☒ | ☐ Human research participants |
| ☒ | ☐ Clinical data |

## Methods

| n/a | Involved in the study |
|---|---|
| ☒ | ☐ ChIP-seq |
| ☐ | ☒ Flow cytometry |
| ☒ | ☐ MRI-based neuroimaging |

## Antibodies

Antibodies used

The following mAb conjugates were used: Name /Clone/ Cat# / Dilution/Manufacture
TCRγσ-FITC GL3 11-5711-82 1:400 Thermo fisher Scientific
TCRγσ-PE GL3 12-5711-82 1:400 Thermo fisher Scientific
TCRβ-FITC H57-597 553171 1:300 BD
TCRβ-PE-Cy5.5 H57-597 560729 1:400 BD
CD4-FITC GK1.5 11-0041-81 1:400 Thermo fisher Scientific
CD4-PE-Cy7 GK1.5 563933 1:500 BD
CD4-allophycocyanin-eFluor780 GK1.5 47-0041-82 1:500 Thermo fisher Scientific
CD8α-allophycocyanin-eFluor780 53-6.7 47-0081-82 1:400 Thermo fisher Scientific
CD8α-allophycocyanin 53-6.7 17-0081-82 1:400 Thermo fisher Scientific
CD8β-PE H35-17.2 550798 1:400 BD
CD8β-PE-Cy7 H35-17.2 25-0083-82 1:400 Thermo fisher Scientific
CD8β-FITC H35-17.2 11-0083-82 1:300 Thermo fisher Scientific
CD19-FITC 1D3 11-0193-82 1:300 Thermo fisher Scientific
CD3ε-FITC 145-2C11 11-0031-82 1:250 Thermo fisher Scientific
B220-PE-Cy7 RA3-6B2 25-0452-82 1:400 Thermo fisher Scientific
CD11C-PE-Cy7 HL3 558079 1:250 BD
CD11b-PE-CY5.5 M1/70 12-0112-81 1:400 Thermo fisher Scientific
MHC-II-allophycocyanin-eFluor780 M5/114.15.2 47-5321-82 1:400 Thermo fisher Scientific
CD64-PE X54-5/7.1 12-0641-80 1:250 Thermo fisher Scientific
CD45-allophycocyanin-eFluor780 30-F11 47-0451-82 1:500 Thermo fisher Scientific
CD45-PE 30-F11 12-0451-82 1:500 Thermo fisher Scientific
CD62L-FITC MEL-14 11-0621-82 1:300 Thermo fisher Scientific
CD122-PE 5H4 12-1221-82 1:400 Thermo fisher Scientific
CD44-allophycocyanin-eFluor780 IM7 47-0441-82 1:400 Thermo fisher Scientific
NK1.1-PE-CY7 PK136 25-5941-82 1:300 Thermo fisher Scientific

CD103-allophycocyanin 2E7 17-1031-82 1:400 Thermo fisher Scientific
FITC-EpCAM G8.8 11-5791-82 1:400 Thermo fisher Scientific

Validation

All antibodies were commercially available in BD or Thermo fisher Scientific and the validation data is available on their websites.

## Eukaryotic cell lines

Policy information about cell lines

Cell line source(s)

293T

Authentication

The cells were from ATCC and not authenticated in our lab.

Mycoplasma contamination

The cells were routinely tested for mycoplasma contamination and found to be negative.

Commonly misidentified lines
(See ICLAC register)

None were used.

## Animals and other organisms

Policy information about studies involving animals; ARRIVE guidelines recommended for reporting animal research

Laboratory animals

Ddx58–/– and Trif–/– mice were provided by Dr. Shizuo Akira (Osaka University). Ddx58–/– mice were backcrossed ten generation to BALB/C background before experiments. Mavs–/– mice were provided by Dr. Jurg Tschopp (University of Lausanne). Mda5–/– mice were provided by Dr. Marco Colonna (Washington University). Tmem173–/– mice were provided Dr. Zhengfan Jiang (Peking University). Cd11c-cre, Villin-cre, Ifnar–/– and Irf1–/– mice were purchased from the Jackson laboratory. TCRδ-GFP mice were provided by Dr. Zhinan Yi (Jinan University). C57BL/6J mice and Rag2–/– mice on a BALB/C background were purchased from Model Animal Research Center. Rig-I-floxed mice were generated by Cyagen Company (Guangzhou, China). Mouse genomic fragments containing homology arms and conditional knockout (cKO) region were amplified from BAC clone by using high fidelity Taq, and were sequentially assembled into a targeting vector together with recombination sites and selection markers. The linearized vector was subsequently delivered to ES cells (C57BL/6J) via electroporation, followed by drug selection, PCR screening, and Southern Blot confirmation. Then ES cells were microinjected into C57BL/6J blastocysts. Chimeric offsprings were backcrossed to C57BL/6J mice, and germline transmission was confirmed by PCR of tail genomic DNA. Founders were confirmed as germline-transmitted via crossbreeding with Flp-deleter. Primers for genotyping of the Ddx58 flox allele were as follows: F1: AGGCCCAAGGATAATTGAAACCC; R1: CTGCCTGGCATCACATCACTAGTT. The use of primers produced bands of 289 bp for the wild-type allele and 417 bp for the Ddx58 flox Neo deleted allele.

Wild animals

Study did not involve wild animals.

Field-collected samples

None.

Ethics oversight

Mice were specific pathogen-free, maintained under a strict 12 hours light cycle (lights on at 07:00 and off at 19:00). All animal experiments were approved by the Ethics Committee of University of Science and Technology of China.

Note that full information on the approval of the study protocol must also be provided in the manuscript.

## Flow Cytometry

### Plots

Confirm that:

☒ The axis labels state the marker and fluorochrome used (e.g. CD4-FITC).

☒ The axis scales are clearly visible. Include numbers along axes only for bottom left plot of group (a 'group' is an analysis of identical markers).

☒ All plots are contour plots with outliers or pseudocolor plots.

☒ A numerical value for number of cells or percentage (with statistics) is provided.

### Methodology

Sample preparation

The small intestine or colon was opened longitudinally and cut into 1-cm-long pieces after removing Peyer's patches. The specimens were washed twice in PBS containing 100 U/ml penicillin and 100 μg/ml streptomycin and then stirred at 37°C in 1×Hank's containing 100 U/ml penicillin, 100 μg/ml streptomycin, and 5% FCS for 30 min. The supernatants were then separated by a 40-70% Percoll density gradient (GE Healthcare), and the cells that layered between the 40-70% fractions were collected as IELs. For LPL isolation, the tissues were shaking in 1×Hank's containing 2 mM EDTA at 37°C for 30 min after IEL isolation. This step was repeated and the supernatants were discarded. The tissues were then digested in 1×Hank's supplemented with 0.5 mg/ml collagenase IV (Sigma-Aldrich) and 10% FCS at 37°C for 20 min. After that, tissues were vortexed vigorously and the suspension were filtered with 70-mm cell strainer. Released cells were then washed in PBS containing 5% FCS and subjected to Percoll fractionation as described above for the isolation of IELs. For IEC isolation, the small intestines were opened longitudinally and cut into 1-cm long pieces. The specimens were washed twice in PBS containing 100 U/ml penicillin and 100 μg/ml streptomycin and then stirred at 37°C in 1×Hank's containing 100 U/ml penicillin, 100 μg/ml streptomycin and 5% FCS for

| | |
|---|---|
| | 30 min. The suspension was filtered with 70-mm cell strainer and the CD45-EpCAM+ IECs were sorted by FACSAria flow cytometer (BD). For isolation of liver mononuclear cells, the murine liver was removed and cut into small pieces, and passed through 70 mm cell strainer. After a 5-min incubation at 4°C, the cells were pelleted and subjected to Percoll fractionation as described above for isolation of IELs. For thymocytes and splenocytes isolation, the organs were directly grinded and suspended in 5 ml PBS containing 5% FBS. For analysis of MLNs and PPs, the organs were cut into small pieces and enzymatically digested with Collagenase IV (0.5 mg/ml, Sigma-Aldrich) at 37°C for 20 min and then filtered prior to analysis. |
| Instrument | BD Verse cytometers, BD FACSAria flow cytometer |
| Software | BD Verse cytometers were used to collected cells and analyzed with FlowJo (v10.0.7) |
| Cell population abundance | For sorting cells, the purity of sorted cells was confirmed within post-sort fractions and regularly maitained >95%. |
| Gating strategy | The gating strategy is explained in supplementary materials. |

☒ Tick this box to confirm that a figure exemplifying the gating strategy is provided in the Supplementary Information.